Restraint Effects in Concrete Bridges

A Study of Cracking due to Thermal Actions and Shrinkage in Portal Frame Bridges

Gottsäter, Erik

2019

Document Version:
Publisher's PDF, also known as Version of record

Restraint Effects in Concrete Bridges

A Study of Cracking due to Thermal Actions and Shrinkage in Portal Frame Bridges

ERIK GOTTSÄTER | FACULTY OF ENGINEERING | LUND UNIVERSITY

Printed by Media-Tryck, Lund 2019 NORDIC SWAN ECOLABEL 3041 0903

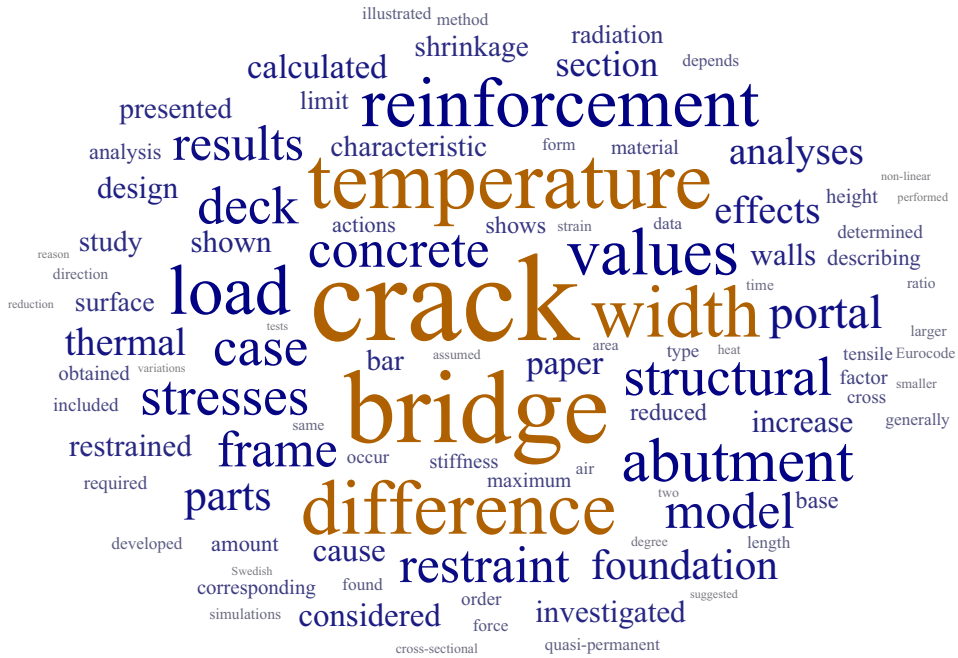

LUND UNIVERSITY

Lund University
Faculty of Engineering
Division of Structural Engineering
Report: TVBK-19/1054
ISSN 0349-4969
ISBN 978-91-87993-14-5

Restraint Effects in Concrete Bridges

A Study of Cracking due to Thermal Actions and Shrinkage in Portal Frame Bridges

Erik Gottsäter

LUND
UNIVERSITY

DOCTORAL DISSERTATION

by due permission of the Faculty of Engineering, Lund University, Sweden.
To be defended in lecture hall V:B in V-huset, John Ericssons väg 1, Lund, at 13.15
on Friday the 29th of November 2019

Faculty opponent
Dr. Mikael Hallgren

Organization: **LUND UNIVERSITY**	Document name: **DOCTORAL DISSERTATION**
Department of Building and Environmental Technology	Date of disputation: **2019-11-29**
Author: **Erik Gottsäter**	Sponsoring organizations: **Trafikverket, SBUF**

Title and subtitle:

Restraint Effects in Concrete Bridges – A Study of Cracking due to Thermal Actions and Shrinkage in Portal Frame Bridges

Abstract

Thermal actions and shrinkage cause volume changes in concrete structures. In structures which are restrained from movements, the restraint effects can cause cracking. However, when cracking occurs, the structure can deform to some extent, which reduces the restraint stresses and thus also the crack widths. As the exact crack development is hard to predict beforehand, the actual restraint and thus also the crack widths are hard to estimate. This makes it difficult to determine the reinforcement required for limiting crack widths to acceptable values. The common design approach does not consider the reduction of restraint due to cracking. Combined with an unclear formulation of the thermal load case for temperature differences between structural parts in bridges, the overestimation of restraint effects that this results in can lead to inefficient use of reinforcement.

In this study, temperature differences between structural parts of portal frame bridges were investigated, in order to suggest a more detailed load case to be used in design of this type of bridges. Temperature simulations of portal frame bridge cross sections and surrounding soil were carried out using finite element modelling. The model used for the simulations was validated by measuring temperature in a bridge and simulating the temperature during the same period of time. Thereafter, it was used to determine new load values, using climate data from different locations in Sweden. Also, crack widths due to thermal actions and shrinkage were investigated using a finite element model with a non-linear material behavior of concrete. In these analyses, the reduction of stiffness due to cracking is included. The model used was validated using test results from previous research.

The thermal load case suggested in this study describes the temperature distribution in the portal frame bridges in a more detailed way than the current load case. It also presents values both for quasi-permanent and characteristic load cases. When comparing the non-linear finite element analysis results with results obtained without including the stress reduction due to cracking, significantly smaller reinforcement amounts were needed for crack width limitation in the non-linear analyses. In the non-linear analyses, the largest crack widths were found to form in the lower part of the abutment, where the effects of the spatial temperature difference and shrinkage difference were coinciding. In the top of the abutment, the crack widths were smaller, but there is a risk that they become larger than the accepted limit, especially if the abutment is thinner than the bridge deck. Cracking due to the investigated restraint effects was however shown to be unlikely in bridge decks of portal frame bridges.

Key words: Restraint, concrete, cracking, thermal action, portal frame bridge, FE-analysis

Classification system and/or index terms (if any)

Supplementary bibliographical information		Language: **English**
ISSN and key title **0349-4969**		ISBN **978-91-87993-14-5**
Recipient's notes	Number of pages: **96**	Price
	Security classification	

Signature:  Date: 2019-10-21

Restraint Effects in Concrete Bridges

A Study of Cracking due to Thermal Actions and Shrinkage in Portal Frame Bridges

Erik Gottsäter

LUND
UNIVERSITY

Cover photography: Bridge no. 12-984-1, a portal frame bridge 0.8 km SW of Värpinge, Sweden. Photo taken 2019-06-24.

Cover illustration back: Frequency of meaningful words in chapters 1–6 of the dissertation.

Faculty of Engineering, Department of Building and Environmental Technology

Report: TVBK-19/1054
ISBN: 978-91-87993-14-5
ISSN: 0349-4969

Printed in Sweden by Media-Tryck, Lund University
Lund 2019

Media-Tryck is an environmentally certified and ISO 14001:2015 certified provider of printed material. Read more about our environmental work at www.mediatryck.lu.se

MADE IN SWEDEN

Preface

The work presented in this thesis was performed during the period 2014 to 2019 at the division of Structural Engineering at Lund University, and to a smaller extent at the division of Structural Engineering at Chalmers University of Technology. The research was financed by Trafikverket, the Swedish Transport Administration (grant number 2013-016) and SBUF, the Swedish construction industry's organization for research and development (grant number 13136).

First of all, I would like to thank my de facto main supervisor, Dr. Oskar Larsson Ivanov, for all of his support and guidance during the process of working with the thesis. I would also like to thank my other supervisors, Dr. Mario Plos, Dr. Miklós Molnár, Prof. Annika Mårtensson and Prof. Roberto Crocetti, for their advice and support. The reference group has also been very helpful in the progress of this project, and I would especially like to thank Dr. Morgan Johansson for his support and passion for this field of research. I would also like to thank my fellow PhD-students and other colleagues for good comradery during my years as a PhD-student.

A special thanks to my parents Gunilla and Anders, as well as my brothers Johan and Mikael, for always being there for me, and I would also like to thank my dear Elin for sharing her life with me and giving me such happiness and joy in my everyday life. Finally, I would like to thank God for the gift of life itself and for caring about us despite our shortcomings.

Sammanfattning

Temperaturändringar och krympning påverkar betongkonstruktioners volym, och i konstruktioner som hindras från av röra sig kan sådana volymändringar leda till så kallade tvångseffekter, som i sin tur kan orsaka sprickbildning. När detta sker kan emellertid konstruktionen deformeras till viss del, vilket gör att tvångsspänningarna och därmed också sprickvidderna minskar. Uppsprickningsförloppet är svårt att förutsäga, och därför blir också tvångskrafterna och sprickvidderna svåra att uppskatta på förhand. Detta gör det svårt att fastslå vilken armeringsmängd som krävs för att begränsa sprickvidderna till acceptabla värden, och i dagens dimensioneringsmetod finns det inget etablerat sätt för hur en minskning av tvångskrafter på grund av uppsprickning ska göras. Kombinerat med en otydlig formulering i lastfall för temperaturskillnader i broar kan detta göra att armeringen i broarna inte utnyttjas optimalt.

I den här studien undersöktes temperaturskillnader mellan konstruktionsdelar i plattrambroar, för att ett mer detaljerat lastfall skulle kunna föreslås för den aktuella konstruktionstypen. Temperatursimuleringar gjordes med en finita-elementmodell av plattrambroar samt intilliggande jord och fyllnadsmaterial. Modellen validerades genom att temperaturen mättes och simulerades i ett givet brotvärsnitt under ett års tid. Därefter användes modellen för att ta fram nya lastvärden med klimatdata från olika platser i Sverige. Dessutom undersöktes sprickvidder orsakade av tvångseffekter med en finita-elementmodell med ett olinjärt materialsamband för dragen betong. Modellen kan beskriva den minskning av tvång som uppsprickningen ger upphov till, och har validerats med hjälp av försök som genomförts i tidigare forskning.

Det temperaturlastfall som föreslås i denna studie beskriver temperaturfördelningen i plattrambroar på ett mer detaljerat sätt än vad som görs i det nuvarande lastfallet, och lastvärden föreslås för både kvasipermanent och karakteristisk lastkombination. De olinjära finita element-analyserna visade att uppsprickning på grund av de undersökta tvångseffekterna är osannolik i broarnas farbaneplattor, men att sprickor däremot kan uppstå både i rambenens ovankant och i nederkant. De största sprickvidderna påträffades vid rambenets nederkant, eftersom effekterna av temperaturlasten och krympningen sammanfaller i detta område.

När resultaten från de olinjära analyserna jämfördes med resultat som togs fram utan hänsyn till den spänningsminskning som uppstår vid uppsprickning sågs stora skillnader i sprickvidd, där sprickvidderna i de olinjära analyserna blev betydligt mindre. Samtidigt var minimiarmeringsmängden otillräcklig för att begränsa sprickvidderna även i de olinjära beräkningarna. Då resultaten också visade att armeringsmängden har en liten påverkan på sprickvidderna i tvångssituationer, kan det vara mer effektivt att minska den ursprungliga tvångsgraden genom att t.ex. ändra brons geometri, än att lägga in extra armering.

Nyckelord: Tvång, betong, uppsprickning, temperaturlast, plattrambro, FE-analys

Abstract

Thermal actions and shrinkage cause volume changes in concrete structures. In structures which are restrained from movements, the restraint effects can cause cracking. However, when cracking occurs, the structure can deform to some extent, which reduces the restraint stresses and thus also the crack widths. As the exact crack development is hard to predict beforehand, the actual restraint and thus also the crack widths are hard to estimate. This makes it difficult to determine the reinforcement required for limiting crack widths to acceptable values. The common design approach does not include the reduction of restraint due to cracking. Combined with an unclear formulation of the thermal load case for temperature differences between structural parts in bridges, the overestimation of restraint effects that this results in can lead to inefficient use of reinforcement.

In this study, temperature differences between structural parts of portal frame bridges were investigated, in order to suggest a more detailed load case to be used in design of this bridge type. Temperature simulations of portal frame bridge cross sections and surrounding soil were carried out using a finite element model. The model was validated by measuring and simulating temperature in a bridge during a one-year period. Thereafter, it was used to determine new load values, using climate data from different locations in Sweden. Also, crack widths due to thermal actions and shrinkage were investigated using a finite element model with a non-linear material behavior of concrete. In these analyses, the reduction of stiffness due to cracking was included. The model used was validated using test results from previous research.

The thermal load case suggested in this study describes the temperature distribution in portal frame bridges in a more detailed way than the current load case. It also presents values both for quasi-permanent and characteristic load cases. In the non-linear analyses, cracking due to the investigated restraint effects was shown to be unlikely in bridge decks of portal frame bridges, but cracks might form both in the top and in the bottom of abutments. The largest cracks were found in the bottom of the abutments, where the effects of the spatial temperature difference and shrinkage were coinciding.

When comparing the non-linear finite element analysis results with results obtained without including the stress reduction due to cracking, significantly smaller reinforcement amounts were needed for crack width limitation in the non-linear analyses. However, the minimum reinforcement amount was insufficient in order to limit crack widths also in the non-linear analyses. As it was also found that the reinforcement amount had a small impact on the crack widths in restraint situations, limiting the initial degree of restraint by e.g. changing the bridge geometry could be a more effective way to reduce the crack widths than to add extra reinforcement.

Key words: Restraint, concrete, cracking, thermal action, portal frame bridge, FE-analysis

Appended papers

Paper I *Comparison of Models for Design of Portal Frame Bridges with regard to Restraint Forces*
Gottsäter E, Larsson Ivanov O, Crocetti R, Molnár M & Plos M.
ASCE Structures Congress 2017, Denver

Paper II *Simulation of thermal load distribution in portal frame bridges*
Gottsäter E, Larsson Ivanov O, Molnár M, Crocetti R, Nilenius F & Plos M.
Engineering Structures, **143**, 219–231 (2017)

Paper III *Validation of Temperature Simulations in a Portal Frame Bridge*
Gottsäter E, Larsson Ivanov O, Molnár M & Plos M.
Structures, **15**, 341–348 (2018)

Paper IV *Spatial Temperature Differences in Portal Frame Bridges*
Gottsäter E & Larsson Ivanov O.
Structural Engineering International (2019)

Paper V *Crack widths in base restrained walls subjected to restraint loading*
Gottsäter E, Johansson M, Plos M & Larsson Ivanov O.
Engineering structures, **189**, 272–285 (2019)

Paper VI *Crack widths in portal frame bridges subjected to restraint effects*
Gottsäter E, Larsson Ivanov O & Plos M.
IABSE Congress 2019, New York

The calculations, analyses and measurements presented in the papers were performed by Erik Gottsäter. Writing the papers and interpreting the results was performed by Erik Gottsäter with valuable assistance from the co-authors.

Notations

Notations used in chapter two:

Notation		Unit
A_{ct}	Concrete cross sectional area in tension	[m^2]
$A_{s,min}$	Minimum reinforcement area	[m^2]
E_s	Reinforcement Young's modulus	[GPa]
$f_{ct,eff}$	Mean concrete effective tensile strength	[MPa]
k	Factor considering non-uniform self-equilibrating stresses	
k_1	Factor considering bond conditions	
k_2	Factor considering strain distribution over cross-sectional height	
k_4	Factor with constant value of 0.425	
k_c	Factor considering strain distribution over cross-sectional height	
k_t	Factor considering load duration	
$s_{r,max}$	Maximum crack spacing at stabilized cracking	[mm]
w_k	Characteristic crack width	[mm]
α_e	Ratio between reinforcement and concrete Young's moduli	
ε_{cm}	Mean concrete strain	
ε_{sm}	Mean reinforcement strain	
$\rho_{p,eff}$	Reinforcement ratio in cross section	
σ_s	Reinforcement stress	[MPa]
φ	Reinforcement diameter	[mm]

Notations used in chapter three:

Notation		Unit
a	Absorptivity	
A_F	Concrete cross sectional area of foundation	[m^2]
$A_{F,max}$	Max concrete cross sectional area of foundation to be considered	[m^2]
A_w	Concrete cross sectional area of wall	[m^2]
E	Young's modulus	[GPa]
E_F	Young's modulus of foundation	[GPa]
E_w	Young's modulus of wall	[GPa]
G	Global radiation	[W/m^2]
h_c	Convection coefficient	[$W/(m^2K)$]

k	Thermal conductivity	[W/(m·K)]
L	Distance	[m]
R	Degree of restraint	
T_{air}	Air temperature	[°C]
$T_{opposite}$	Temperature of opposite surface	[°C]
T_s	Surface temperature	[°C]
T_{sky}	Sky temperature	[°C]
q	Heat flux	[W/m^2]
q_c	Heat flux due to convection	[W/m^2]
q_r	Heat flux due to long wave radiation	[W/m^2]
q_s	Heat flux due to solar radiation	[W/m^2]
q_{sky}	Incoming long wave radiation from the sky	[W/m^2]
v	Wind speed	[m/s]
α	Coefficient of thermal expansion	
ΔT	Temperature change/difference	[°C]
ε	Emissivity	
ε_R	Restraint strain	
ε_{tot}	Total strain, restrained + unrestrained	
σ	The Stefan-Boltzmann constant	[W/(m^{2}K^4)]
σ_R	Restraint stress	[MPa]

Notations used in chapter four:

Notation		**Unit**
A	Area	[m^2]
A_c	Concrete area	[m^2]
A_{eff}	Effective concrete area	[m^2]
$A_{I,eff}$	Stage I effective concrete cross sectional area	[m^2]
A_s	Reinforcement area	[m^2]
E	Young's modulus	[GPa]
E_c	Concrete Young's modulus	[GPa]
$E_{c,eff}$	Young's modulus with consideration to creep	[GPa]
E_I	Stage I Young's modulus	[GPa]
E_{II}	Stage II Young's modulus	[GPa]
E_s	Reinforcement Young's modulus	[GPa]
F	Force	[kN]
f_{cm}	Mean concrete compressive strength	[MPa]
f_{ct}	Concrete tensile strength	[MPa]
F_I	Stage I force	[kN]
F_{II}	Stage II force	[kN]

F_R	Restraint force	[kN]
H	Height	[m]
k	Spring stiffness	
L	Length	[m]
l_t	Transmission length	[mm]
R	Degree of restraint	
s	Slip	[mm]
w_m	Mean crack width	[mm]
w_k	Characteristic crack width	[mm]
α	Coefficient of thermal expansion	
ΔL	Elongation	[m]
ΔL_R	Restrained elongation	[m]
ΔT	Temperature change	[°C]
ε	Strain	
ε_{cm}	Mean concrete strain	
ε_{free}	Strain if element were unrestrained	
ε_R	Restraint strain	
ε_{sm}	Mean reinforcement strain	
σ_c	Concrete stress	[MPa]
σ_s	Reinforcement stress	[MPa]
τ_b	Bond stress	[Pa]
φ	Reinforcement diameter	
ϕ	Creep coefficient	

Contents

1 Introduction

1.1 Background

Temperature variations and shrinkage affect the volume and shape of reinforced concrete structures. Both concrete and reinforcement changes volume due to temperature variations, while shrinkage affects the concrete volume only. If the changes of shape and volume induced by temperature and shrinkage are prevented, either by the surroundings or by the structure itself, restraint stresses appear in the structure. Restraint stresses can cause cracking in reinforced concrete, which in turn may decrease the structural durability. It is therefore important to consider thermal actions and shrinkage in design of reinforced concrete structures.

In the present Eurocode, several thermal load cases are given, which shall be considered in design of bridges. One of these load cases prescribes a difference in temperature of 15°C between "main structural elements". The load case is in Sweden considered in design of e.g. portal frame bridges, and the temperature difference prescribed in the load case is applied between the bridge deck and the abutments, as well as between abutments and foundations.

If a 2D frame model of the bridge is used in design, as was previously the case, the load case does not cause any significant effects on the structure. However, since 2011 the Swedish Transportation Administration states that 3D models describe the functionality of bridges properly, while 2D models only do the same in cases where two dimensions are sufficient to describe e.g. the geometry and loading (Trafikverket, 2011b). This lead to 3D models being used in design of most bridge types in Sweden. In the 3D models, the effect of the load case in the transverse direction is also considered. In this situation, the prescribed thermal load case can indicate large tensile stresses in the transverse direction of portal frame bridges particularly, since linear elastic material properties are generally used. Shrinkage can also contribute to the tensile stresses in the transverse direction if casting is made in different stages, allowing for the parts cast first to shrink before the casting of the other parts. However, the stress levels in the design model depend on the interpretation and implementation of the thermal load case, which can vary between different bridge designers.

The larger stress values obtained when using 3D models instead of 2D models resulted, in many cases, in a drastic increase in reinforcement amount in the bridges. However,

as existing bridges had not been reported to suffer from cracking due to these load effects to any great extent, the results were suspected of being inaccurate. Comparisons of bridges built in Sweden have also showed that the reinforcement amounts used in bridge construction have increased substantially during the time period from approximately 1970 to 2000 (Bygginovationen, 2010). As the older bridges are generally considered to have a sufficient durability, the increase in reinforcement could be partly unnecessary from a durability point of view.

In order not to prescribe unnecessary reinforcement when considering restraint effects, bridge designers have come up with different approaches to obtain a result that renders similar reinforcement amounts as when 2D models were used, while still abiding by the new design rules. This can be achieved by e.g. reducing the Young's modulus of the concrete in the design model, assuming that the temperature varies linearly over the entire height of the abutment, or assuming that all concrete is unstressed due to cracking, and restraint effects thus only develop in the reinforcement. However, there is a lack of consensus regarding the reasonableness of the various interpretations of the thermal load case, and the methodology in treating the restraint effects when calculating crack widths. This is considered problematic in the field of bridge engineering in Sweden. One problematic scenario is e.g. if the reviewer of a set of calculations has a differing opinion than the designer regarding how to handle the issue, while none of them have any scientific data to motivate their standpoint.

1.2 Objectives

The objective of this research project is to investigate cracking due to restraint effects caused by thermal actions and shrinkage. This includes the following:

- To investigate the spatial temperature variations within portal frame bridges, and the possible differences in temperature between structural parts.
- To propose a new way to consider the load case with temperature differences between structural parts of portal frame bridges in design situations.
- To investigate crack widths when cracking is caused by restraint effects, considering the reduction of restraint stresses due to cracking.
- To investigate the possibilities for a new way to consider the reduction of restraint stresses due to cracking in design situations, without having to perform non-linear analyses.

1.3 Scientific approach and methodology

The scientific approach used in this study included literature reviews, field measurements, analytical calculations and numerical analyses. Finite element (FE) simulations using a model first presented in Larsson (2009) were performed in order to investigate the spatial temperature differences in the bridges. Weather data obtained from SMHI, the Swedish Meteorological and Hydrological Institute, was used in the simulations, and parametric studies using the fractional factorial method were performed in order to investigate the influence of various parameters on the result.

The model for temperature simulation was validated for use on portal frame bridge cross sections, as the model had not been used in this type of structure previously. The validation was performed by measuring the temperature in 12 points in a portal frame bridge cross section during a one-year period, and comparing the results with simulated temperature. The air temperature data used in the simulation was measured on site, while radiation was measured about 5 km away from the bridge and wind speed was taken from a weather station operated by SMHI about 15 km away from the bridge.

The simulation performed in the validation also showed that the temperature difference between abutment and foundation could be larger than the difference between bridge deck and abutment. This temperature difference had previously not been considered within the study, but was thereafter also investigated. After having verified the model, long-term simulations were made using all eight available data series from SMHI with at least 10 years of data. The number of series is limited by the long-wave radiation, which is measured at only a few locations in the country. Thereafter, the general extreme value distribution was used to analyze the data and suggest characteristic and quasi-permanent load values for the temperature differences.

Crack widths resulting from restraint effects were initially investigated analytically for simple geometrical cases. As these methods were difficult to apply to more complicated geometries, such as base restrained walls, an FE-analysis model using a non-linear material model for concrete and a bond-slip interaction for concrete to reinforcement interaction was developed. The model was verified using test results presented in previous research, and was thereafter applied to portal frame bridges. The verification of the model by analyzing base restrained walls was chosen as, to the author's knowledge, no investigation of cracking due stresses in the transverse direction of portal frame bridges which could be used to verify the model have been performed. However, portal frame bridges are similar to base restrained walls when the transverse direction is considered. After verifying the model, the suggested thermal load case was applied, and the resulting cracking was investigated for different use of reinforcement and bridge geometries.

1.4 Limitations

The study investigated thermal actions for Swedish climate, i.e. using weather data from Sweden only. The results can be applied to other areas with similar climate, but the load values could be improper if used in a region with differing climate. Only thermal stresses due to differences in temperature between structural parts have been investigated, and the load values were determined using series of climate data from eight different locations within the country. Only one-span portal frame bridges with roads underneath (i.e. no running water) were investigated.

Crack widths were mainly investigated in the quasi-permanent load combination, and to some extent also in characteristic load combination. The focus is on the quasi-permanent load combination as this load combination is used for crack width limitation in design situations. Only self-weight, vertical earth pressure, thermal actions and shrinkage have been included in the analyses, as these were the only loads considered necessary to include in order to describe the stresses in transverse direction of the bridges. Also, the wing walls have been omitted from the analyses. Furthermore, only a limited number of analyses were performed, especially with regards to geometrical variations.

1.5 New findings

The main findings of the performed study presented in this dissertation are:

- When simulating temperature in portal frame bridges, the parameters having the largest influence on temperature differences between bridge deck and abutment are the thickness of the structural parts and the asphalt heat conductivity and absorptivity. (paper II)
- The model for temperature simulation in portal frame bridges presented in this dissertation can be used to re-create temperatures in bridges. When investigating temperature differences between structural parts, the accuracy of the model is high, while the precision is somewhat lower. For this reason, a 1.5°C error margin can be added if the temperature at a specific time is of interest, while no error margin is needed if the average over long time is of interest. (paper III)
- A characteristic load value of 15°C was found for temperature differences between bridge deck and abutment, while 27°C was found for characteristic temperature differences between abutment and foundation. For the difference between bridge deck and abutment, the highest values were based on climate data from Lund, which is situated in the south of Sweden. This was due to the

larger influx of solar radiation in the south of the country. The difference between abutment and foundation was however based on results using climate data from Kiruna, in the north of Sweden. This temperature difference was found to be governed by the seasonal temperature variations to a larger extent. Reasonable corresponding quasi-permanent load values were found to be 4°C and 7°C, respectively. (paper IV)

- The non-linear FE-model developed in the study was found to re-create cracking in base restrained reinforced concrete walls with an acceptable margin of error, and tended to overestimate cracking and crack widths, which is preferable. (paper V)
- Cracking in the bridge deck due to the investigated restraint effects is found to be unlikely. In the top of the abutment, the crack widths can be expected to be small, unless the cross-sectional height of the abutment is smaller than that of the bridge deck. The largest cracks are however likely to form in the lower part of the abutment. (chapter 4)
- When using the new thermal load case and a difference in shrinkage between structural parts in non-linear FE-analyses of a specific bridge geometry, the reinforcement amount required for crack width limitation was found to be 57% less than when using linear elastic material model and a conservative interpretation of the Eurocode load case. (paper VI) However, the relation between crack width and the magnitude of the applied thermal action and shrinkage is more complicated than in non-restraint cases, as the restraint effects are reduced by cracking. Also, the reinforcement amount seems to have a smaller influence on the crack width in restraint cases. (chapter 4)

1.6 Outline of dissertation

This dissertation is divided into seven chapters which are presented below. After these chapters, the academic research papers which this dissertation is based upon are appended. These papers constitute of four journal papers and two conference papers.

- Chapter two gives an introduction to portal frame bridges, and design of portal frame bridges, with the focus on the reinforcement amount required for crack width limitation.
- Chapter three describes the concept of restraint, and how thermal actions and shrinkage can cause restraint effects in reinforced concrete structures. The occurrence of thermal actions in bridges is described, and the conclusions from the study of temperature differences between structural parts in portal frame bridges within this research project are also presented.

- Chapter four describes cracking in reinforced concrete, focusing on restraint situations. Methods to calculate cracking analytically in end-restrained specimens are presented, and the FE-model used to investigate cracking in base restrained walls is introduced. Results from using this model for analysis of cracking in portal frame bridges are also shown, and compared with results obtained with the conventional method of today, which do not include the stress reduction due to cracking.
- Chapter five summarizes the papers appended to this dissertation.
- Chapter six presents the main conclusions from the PhD-project, and also suggests ideas for further research.
- Chapter seven contains the reference list.

2 Portal frame bridges

The portal frame bridge is the most common bridge type in Sweden. The Swedish transport administration, has as of 2019-05-06 over 7500 portal frame bridges listed in their database of Swedish bridges and tunnels, BaTMan (Trafikverket, 2018), of a total of 20800 bridges. Of the portal frame bridges in the database, half were constructed before 1973, and the decade during which most were constructed is the 1950s.

Portal frame bridges are built in reinforced concrete, and consist of a bridge deck carried by two abutments which in turn are placed on foundations. Wing walls are usually placed on the side of the abutments, in order to keep the soil on place. Fig. 2.1 shows an example of a portal frame bridge, and Fig. 2.2 shows a sketch of the bridge, with the structural parts marked out. The figure also shows a definition of directions used in this dissertation. An illustration of a portal frame bridge cross section is shown in Fig. 2.3. The bridge deck consists of a reinforced concrete slab, which carries the loads on the deck without requiring any beams underneath. The deck is rigidly connected to the abutments, which in turn are rigidly connected to their respective foundations.

Fig. 2.1. A portal frame bridge.

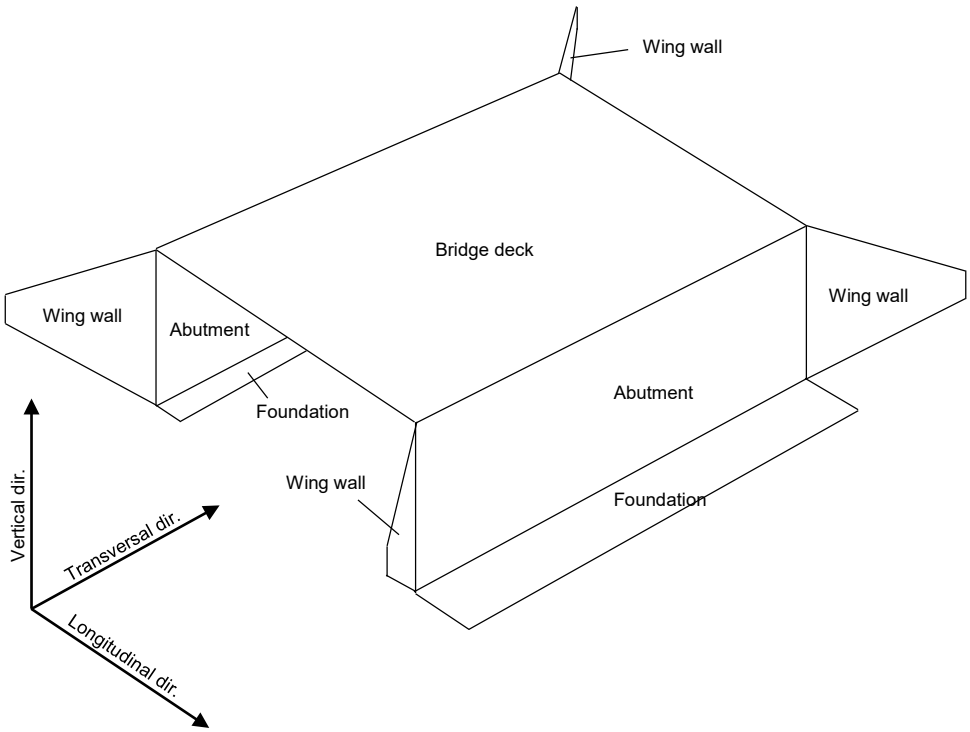

Fig. 2.2. Sketch of a portal frame bridge.

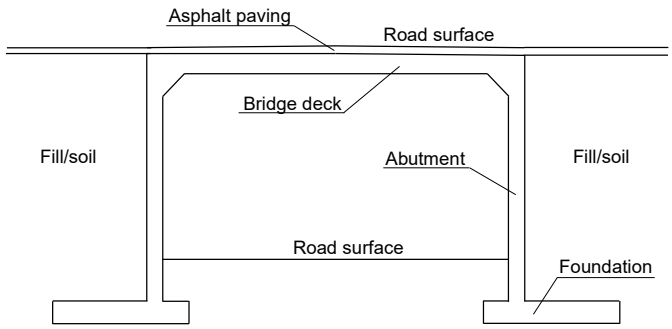

Fig. 2.3. Example of a portal frame bridge cross section.

The span lengths of portal frame bridges can be up to 35 m, but spans over 22–25 m require the use of prestressed reinforcement. Some variations in geometry are possible, e.g. bridges with small spans and bridges placed on soil with poor load carrying capacity can have a single large foundation, instead of separate foundations for the two abutments. Also, if the bridge is long, extra supports can be placed in e.g. mid-span (Vägverket, 1993). Expansion joints are not used in the structural type.

Portal frame bridges are cast in place, and the rigid connections between the structural parts are achieved by connecting the parts with reinforcement. The bridges are usually cast in two stages, the foundation in a first stage, and then the abutments and bridge deck in a second stage. The abutments are thus cast directly on the foundations, and the abutments and bridge deck are cast as one entity, with generally only a 1–2 hour pause in the casting process after between casting the abutment and bridge deck. This pause in casting was previously explicitly required by the Swedish transport administration (Vägverket, 1994).

2.1 Design of portal frame bridges

Swedish bridges are designed after the regulations in Eurocode. Eurocode describes the design methodology and definition of load combinations (Eurocode 0, CEN (2002)), as well the description of specific loads (Eurocode 1, e.g. CEN (2003)), load effects and the capacity of structural members (Eurocode 2, e.g. CEN (2005a) and CEN (2005b)). In addition, the Swedish Transport Administration publishes national choices regarding bridge structures (e.g. Trafikverket (2011a)), as well as national documents on design calculations and practical execution (Trafikverket, 2016a), (Trafikverket, 2016b).

In Sweden, bridges are generally designed using 3D finite element (FE) analyses. The use of 3D models is required by the Swedish Transport Administration (Trafikverket, 2011b, Trafikverket, 2016b), but previous to this demand, portal frame bridges were generally designed using 2D frame models. The reinforcement placed in the transversal direction was in such cases not calculated considering the load effects on the bridge. Instead, minimum reinforcement (see section 2.1.2) was placed in the transverse direction. Along edges between structural parts where differences in shrinkage could be expected, a standardized amount of extra reinforcement, (5φ16 on each side of the cross section) was placed, which is still prescribed today (Trafikverket, 2016b).

In the 3D analyses used in design of portal frame bridges in Sweden today, the concrete is given a linear elastic material behavior. This means that cracking cannot occur in the analyses, and the reinforcement can therefore be omitted from the models. Instead, the required reinforcement amounts are calculated from the tensile forces and bending moments obtained in the analyses. Analyses with non-linear material models for concrete are generally not used in design, as the final structure, including the reinforcement, must be assumed beforehand in such analyses. Also, load effects cannot be superimposed, and the calculation procedure is more complicated, meaning that convergence issues often arise. Furthermore, many material parameters, which are often unknown, must be specified.

Several different types of loads are to be considered in bridge design, e.g. self-weight, traffic loads, earth pressure, shrinkage and thermal actions. Different limit states are used in design. In order to verify that the bridge has a sufficient load carrying capacity, the loads are combined in ultimate limit state and compared with the calculated design load carrying capacity of the structure. There is also a serviceability limit state, which is used to verify demands regarding e.g. deformations and cracking. This study focuses on the demands regarding cracking in serviceability limit state. As restraint stresses are reduced by cracking (see chapter 4), which normally is extensive in the ultimate limit state, restraint effects are often omitted un ultimate limit state.

The demands regarding cracking in concrete structures are verified by calculating the crack widths caused by a quasi-permanent load combination, in which the included load magnitudes shall generally correspond to the mean or average value over time. The load values in Eurocode 1 are generally given as characteristic load values, i.e. load values which have a return period of 50 years. In order to obtain quasi-permanent load values, the characteristic load values are multiplied with ψ_2-factors. For permanent loads such as self-weight and shrinkage, the factor equals 1, but for variable loads, the factor value is smaller. The ψ_2-factor for thermal actions is e.g. 0.5, and the factor equals zero for traffic loads (CEN, 2002).

2.1.1 Crack width limitation

Eurocode states demands on maximum allowable crack widths in order to assure durability, and for aesthetic reasons. In Sweden, national choices have been made which limit characteristic crack widths in bridges with design working life of 100 years to 0.2 mm, or 0.15 mm for surfaces exposed to chlorides, such as de-icing salts. The crack widths are calculated from the reinforcement stress using Eqs. (2.1–2.3), which are presented in section 7.3.4 in Eurocode 2 (CEN, 2005a). The factors in the equations are defined in Table 2.1. Eq. (2.2) is adapted after the Swedish national choice for the equation (Trafikverket, 2011a).

$$w_k = s_{r,max}(\varepsilon_{sm} - \varepsilon_{cm}) \tag{2.1}$$

$$s_{r,max} = 7\varphi + k_1 k_2 k_4 \varphi / \rho_{p,eff} \tag{2.2}$$

$$(\varepsilon_{sm} - \varepsilon_{cm}) = \frac{\sigma_s - k_t \frac{f_{ct,eff}}{\rho_{p,eff}}(1+\alpha_e \rho_{p,eff})}{E_s} \geq 0.6\frac{\sigma_s}{E_s} \tag{2.3}$$

Table 2.1. Definitions of factors used in Eqs. (2.1–2.3).

Factor	Description	Value
w_k	Characteristic crack width	
$s_{r,max}$	Maximum crack spacing at stabilized cracking	
ε_{sm}	Mean reinforcement strain along the distance $s_{r,max}$	
ε_{cm}	Mean concrete strain along the distance $s_{r,max}$	
φ	Reinforcement diameter	
k_1	Factor considering bond conditions	0.8 for bars with ribs
k_2	Factor considering strain distribution over cross sectional height	0.5 if pure bending and 1.0 if pure tension
k_4	Factor with constant value	0.425
$\rho_{p,eff}$	Reinforcement ratio in cross-section	Reinforcement cross-sectional area divided by effective concrete cross-sectional area
σ_s	Reinforcement stress in cracked section	
k_t	Factor considering load duration	0.6 for short term loading and 0.4 for long term loading
$f_{ct,eff}$	Mean concrete tensile strength at time of cracking	Depends on concrete quality
α_e	Ratio between reinforcement and concrete Young's moduli	Depends on concrete quality and load duration (i.e. creep)
E_s	Reinforcement Young's modulus	200 GPa

As reinforcement is not included in the general FE-analyses used in design, Eqs. (2.1–2.3) can instead be used to find the maximum allowable reinforcement stress in cracked sections given the demand on crack widths. The maximum allowed reinforcement stress in combination with the tensile forces and bending moments obtained from the FE-analyses can thereafter be used to determine the required reinforcement cross-sectional area in a given cross section of the bridge.

2.1.2 Minimum reinforcement

In structural parts where tensile stresses might appear, the reinforcement amount must not be smaller than the minimum reinforcement, described in section 7.3.2 of Eurocode 2 (CEN, 2005a). The introduction of the minimum reinforcement area guarantees that the reinforcement stress after cracking is lower than the yield stress. This means that more cracks will form before failure is reached, i.e. the total crack width will be distributed over several cracks, which is important in order to assure ductility. The expression for the minimum reinforcement amount, denoted $A_{s,min}$, is given in Eq. (2.4), and the factors are defined in Table 2.2. Additional demands for minimum reinforcement in Swedish bridges are found in Trafikverket (2016a) and Trafikverket (2016b).

$$A_{s,min} = k_c k f_{ct,eff} A_{ct} / \sigma_s \tag{2.4}$$

Table 2.2. Definitions of factors used in Eq. (2.4).

Factor	Description	Value
$A_{s,min}$	Minimum reinforcement amount	
k_c	Factor considering strain distribution over cross sectional height	1.0 if pure tension
k	Factor considering non-uniform self-equilibrating stresses	For portal frame bridges, the value depends on the cross-sectional height of the structural parts
$f_{ct,eff}$	Mean concrete tensile strength at time of cracking	Depends on concrete quality
A_{ct}	Concrete cross sectional area in tension	
σ_s	Maximum permitted tensile stress in reinforcement after crack formation	Usually the characteristic yield stress

3 Restraint stresses in portal frame bridges

3.1 The concept of restraint

Restraint stresses are stresses which appear when a structural element is prevented from obtaining its desired shape and volume. As shrinkage and thermal actions, described more in detail in sections 3.2 and 3.3, causes a desire to change the shape and volume, these actions will cause restraint stresses if the desired movements are prevented.

Two simple cases of restrained structures are end-restrained bars and base restrained (or edge restrained) walls, as illustrated in Fig. 3.1. If these structures are subjected to e.g. a decrease in temperature, this will cause a desire to contract in the horizontal direction, which will be fully or partly prevented by the restraining conditions. This will in turn cause restraint stresses to appear in the structures, which can be calculated using Hooke's law, see Eq. (3.1). In the equation, σ_R is the restraint stress, ε_R is the restrained strain and E is Young's modulus (Engström, 2014), (Jokela, 1984).

$$\sigma_R = \varepsilon_R E \tag{3.1}$$

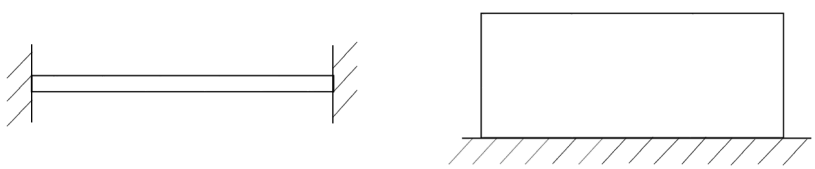

(a) (b)

Fig. 3.1. Illustration of an end restrained bar (a) and an edge restrained wall (b).

In the end-restrained structure, the magnitude of the restraint stress in horizontal direction will be uniform in the structure. However, the horizontal restraint stresses will vary within the edge-restrained wall, due to e.g. a smaller part of the desired strain being prevented in the top of the wall than in the bottom. In order to describe how large part of the desired strain that is restrained, the degree of restraint, R, is used, which is defined in Eq. (3.2). In this context, the desired strain, ε_{tot}, is the strain that would occur if no restraint was present, and the structure could contract freely. The restrained

strain, ε_R, is on the other hand the strain which is prevented from forming (Engström, 2007).

$$R = \frac{restrained\ strain}{desired\ strain} = \frac{\varepsilon_R}{\varepsilon_{tot}} \tag{3.2}$$

For an end-restrained bar as in Fig. 3.1 (a), the degree of restraint will thus equal 1 in the entire bar if the edges are completely rigidly connected. However, in the base-restrained wall in Fig. 3.1 (b), the degree of restraint will vary, which is illustrated in Fig. 3.2, as the wall is only restrained along one edge. The variation of the degree of restraint in the wall is dependent on the geometry of the wall. If e.g. the length of the wall increases in relation to the height, the influence of the restraining edge will increase, and the degree of restraint will thus generally also increase.

The maximum degree of restraint depends on the stiffness ratio of the connected structural parts, and is in most practical cases smaller than 1. The maximum degree of restraint, forming along the bottom edge of a base restrained wall, can be estimated using Eq. (3.3), presented in ACI Committee 207 (1990). A_w and A_F are the cross sectional area of the wall and the foundation respectively, and E_w and E_F are the corresponding Young's moduli. In practice, the area of the restraining body is limited to $A_{F,max} = 2.5A_w$, as only the closest part of a large foundation is effectively reducing the contraction of a wall (ACI Committee 207, 1990).

$$R = \frac{1}{1+\frac{A_W E_W}{A_F E_F}} \tag{3.3}$$

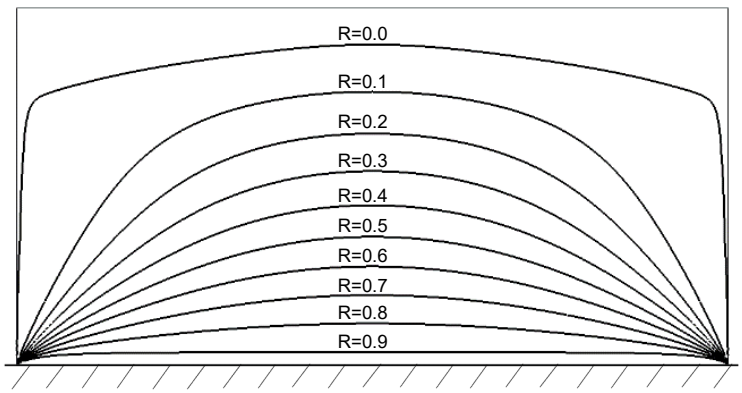

Fig. 3.2. Example of degree of restraint, *R*, in the horizontal direction of a base restrained wall with length / height = 2 and *R=1* along the bottom edge.

In portal frame bridges, the bridge deck and abutments are rigidly connected, as well as the foundations and the abutments. For a portal frame bridge as illustrated in Fig. 2.2, the degree of restraint will be vastly different in the different directions. This

was shown in paper VI, where the degree of restraint in a given bridge was found to be 0.01 in the longitudinal direction (see Fig. 2.2) in the bridge deck, and 0.5 in the transversal direction (see Fig. 2.2) along the edge between bridge deck and abutments. There is also a significant restraining effect along the edge between the abutments and foundations. This effect was not investigated in that study, but it can be estimated for a given geometry e.g. by using Eq. (3.3) or by performing FE-analyses.

The larger degree of restraint in the transversal direction corresponds to the base restrained case, as the restraint is caused along one edge of the rectangular structural parts. Restraint stresses can appear in the transversal direction of the structure due to thermal actions and shrinkage, which are described in section 3.2 and 3.3, respectively. Fig. 3.3 shows an example of restraint in the transversal direction of a portal frame bridge. In the figure, the bridge deck is subjected to a uniform decrease in temperature, $-\Delta T$, while the temperature in the abutments is unchanged and the foundations are subjected to a uniform increase in temperature, ΔT. The figure illustrates the degree of restraint, i.e. to how large extent the desired movements due to the temperature changes are prevented. In this case, the restraint will cause tensile stresses in the bottom of the abutments and in the bridge deck. If instead the bridge deck was warm and the foundations were cold, tensile stresses would appear in the top of the abutments and in the foundations.

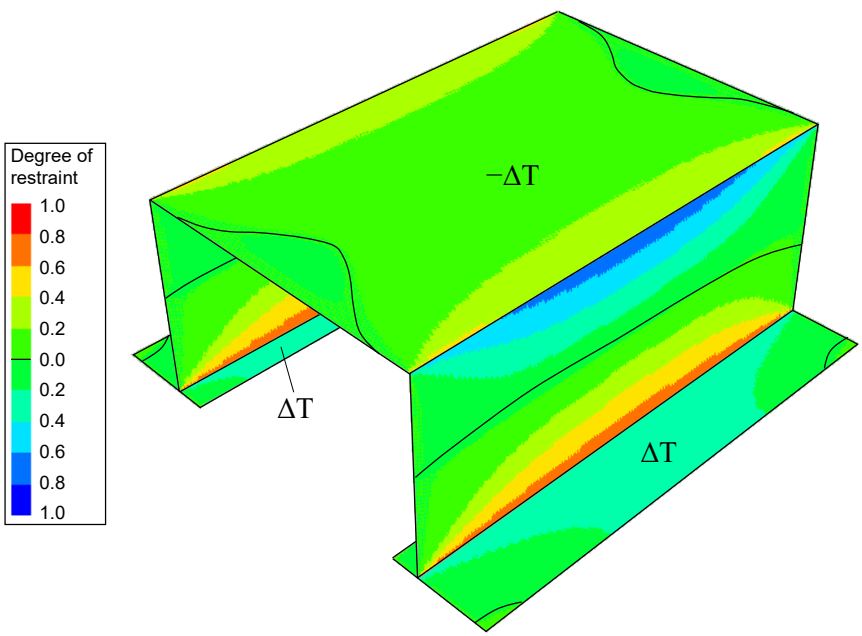

Fig. 3.3. Degree of restraint in portal frame bridge, when subjected to a uniform temperature increase ΔT in the foundations and a uniform temperature decrease $-\Delta T$ in the bridge deck.

3.2 Thermal actions in portal frame bridges

When the temperature of concrete and reinforcement changes, the volume of the materials is affected. These desired volume changes can lead to restraint stresses, if the volume changes are prevented by e.g. surrounding structures or structural parts. The change in volume is described by the coefficient of thermal expansion, α, which multiplied with the change in temperature, ΔT, gives the strain caused by ΔT. For concrete, the value of the coefficient of thermal expansion depends on the cement to aggregate ratio, the type of aggregate and the degree of water saturation. The coefficient is in the range of $5.4{\cdot}10^{-6}$ °C^{-1} to $14.2{\cdot}10^{-6}$ °C^{-1}, where the lower value represents a water saturated concrete with low cement ratio (200 kg/m^3) and limestone-based aggregate, whereas the higher value represents an air dried concrete with a high cement ratio (600 kg/m^3) and a quartz-based aggregate (Ljungkrantz et al., 1994). fib Model Code 2010 (fib, 2013) presents a slightly different range, stating that the concrete coefficient of thermal expansion is between $6{\cdot}10^{-6}$ °C^{-1} and $15{\cdot}10^{-6}$ °C^{-1}. The same source also states that $10{\cdot}10^{-6}$ °C^{-1} should be used in design, which is also stated in Eurocode 1 (CEN, 2003). The reinforcement coefficient of thermal expansion can also be assumed to be $10{\cdot}10^{-6}$ °C^{-1} (fib, 2013), (Ljungkrantz et al., 1994), (CEN, 2003). It is thereby generally assumed that the two materials desire the same volume change when subjected to thermal actions. In papers I, II and III, a coefficient of thermal expansion equaling $10{\cdot}10^{-6}$ °C^{-1} was used for both materials.

3.2.1 Heat transfer

Heat transfer is what causes changes in temperature over time, and it occurs whenever there are temperature differences within of between objects. It can occur in three different forms: conduction, convection and radiation, and the total heat flux is determined by the combined effect of these forms of heat transfer.

Conduction describes heat being transferred directly between two molecules in contact with each other, and it thereby occurs within a medium or between two media which are adjacent to each other. For two parallel surfaces with different temperature and with a homogenous material in between, the heat flux q in [W/m^2] through the homogenous material can be expressed as in Eq. (3.4), where ΔT is the temperature difference and L is the distance between the surfaces. k is the thermal conductivity of the material, often given in [W/(m·K)] (Incropera et al., 2007).

$$q = k\frac{\Delta T}{L} \tag{3.4}$$

The thermal conductivity of concrete is often in the range of 1.6–2.5 W/(m·K), and depends on the density and moisture content, as well as the thermal conductivity of the

cement and aggregate (Ljungkrantz et al., 1994). For asphalt, the aggregate type used as well as the proportion of bitumen, which has a lower thermal conductivity than the aggregate, are governing factors. The conductivity of asphalt is generally in the range of 0.7–2.5 W/(m·K) (Larsson, 2012). For soil, the thermal conductivity can vary from about 0.4 W/(m·K) in a dry friction soil to about 1.1 W/(m·K) in a water saturated clay with low porosity (Sundberg, 1991). In papers II, III and IV, the thermal conductivity of the materials was assigned values within the respective ranges. In paper II, a parametric study was performed, in which the effect of varying the thermal conductivity of the materials within the respective ranges was investigated.

Convection can occur if there is a temperature difference between a gas or a liquid and an adjacent surface. A common example is convection between air and ground. In this case, if the ground is warmer than the air, the air adjacent to the ground will heat up due to conduction. This in turn affects the density of the air, which makes the warmer molecules rise and be replaced by colder molecules. This mixing of the medium thus increases the temperature difference over the surface, which in turn increases the conduction (Kreith, 1973). However, convection along surfaces facing air is often greatly affected by the wind speed, as the wind significantly increases the mixing of the molecules in the air. The heat flux due to convection over a surface facing air is dependent on the convection coefficient, h_c, the surface temperature, T_s and the air temperature, T_{air}, as shown in Eq. (3.5).

$$q_c = h_c(T_s - T_{air}) \tag{3.5}$$

The convection coefficient, h_c, in [W/(m^{2}K)] can be calculated from the wind speed v according to expressions given by Nevander and Elmarsson (2006), shown in Eqs. (3.6–3.7), which were used in papers II, III and IV.

$$h_c = 6 + 4v, \ v \leq 5\ m/s \tag{3.6}$$

$$h_c = 7.4v^{0.78}, \ v > 5\ m/s \tag{3.7}$$

Radiation describes heat transfer between objects separated by a transparent medium or by vacuum. The radiated energy can be described as an electro-magnetic wave, whose wavelength depends on the temperature of the surface of the emitting body (Duffie and Beckman, 2006). All surfaces emit this type of radiation, but it is often divided into two types in temperature simulations, namely solar radiation (or short-wave radiation) and long-wave radiation. Solar radiation is absorbed by all surfaces that are reached by sunlight. Thermal flux from solar radiation is calculated using Eq. (3.8) as the absorptivity of the material, a, multiplied by the incoming solar radiation, G. The absorptivity is thus a factor in the range from zero to one, describing the proportion of the energy being absorbed (Kreith, 1973).

$$q_s = aG \tag{3.8}$$

The solar absorptivity depends on the surface color, as darker surfaces absorb more light than brighter surfaces. For asphalt, the absorptivity is often in the range of 0.8–0.95, where the higher value corresponds to newly placed asphalt. As the asphalt ages, oxidation causes the bitumen to fade, which makes it brighter (Bretz et al., 1997). Concrete is a brighter material than asphalt and thus has a lower absorptivity, which can be assumed to be in the range of 0.5–0.78 (Larsson, 2012). Concrete paving will thereby absorb less solar radiation than asphalt paving. As more absorbed heat in the bridge deck enables larger temperature differences between the deck and the abutment, only asphalt paving was used in papers II, III and IV. The absorptivity was assigned values within the presented range for asphalt, and the effect of varying the absorptivity was also investigated in paper II.

The wave length of the emitted radiation increases with decreasing temperature. In this study, long wave radiation is defined as all radiation not originating from the sun. As the application regards temperature in bridges, this includes radiation emitted by the surface of the bridge structure and by the ground underneath it. It also includes incoming radiation from the sky, from e.g. clouds and stars as solar radiation is excluded.

As all surfaces emit radiation, and the emitted radiation increases with increasing temperature, the net radiation will go from the warmer surface to the colder. Heat flux due to long wave radiation is determined by the Stefan Boltzmann law shown in Eq. (3.9), where σ is the Stefan-Boltzmann constant of $5.67 \cdot 10^{-8}$ W/(m^2°C^4), ε is the emissivity of the surface material, T_s is the surface temperature and $T_{opposite}$ is the temperature of the opposite surface. The emissivity is a factor between zero and one, depending on the characteristics of the surface layer, and describing to what extent the surface is emitting long-wave radiation (Larsson, 2012).

$$q_r = \sigma\varepsilon\left(T_s^4 - T_{opposite}^4\right) \tag{3.9}$$

For long wave radiation, the absorptivity is equal to the emissivity of the material. For this reason, Eq. (3.9) only includes the emissivity. Concrete emissivity varies between 0.85 and 0.95 (Threlkeld, 1970), and was set to 0.9 in Larsson (2009). The emissivity of asphalt is similar to the concrete emissivity, as shown by e.g. Quinn Brewster (1992) who assigns the value 0.93 to asphalt and 0.94 to concrete. Branco and Mendes (1993) used 0.9 for both materials, which was also used in papers II, III and IV. Paper II also investigated the effect of varying the emissivity from 0.85 to 0.95.

Eq. (3.9) shows how net long wave radiation can be calculated from the temperature of surfaces. However, such a temperature cannot be determined directly for the sky. Instead, a corresponding sky temperature must first be determined from measurements

of incoming long wave radiation, using Eq. (3.10). In the equation, q_{sky} is the incoming long wave heat flux and T_{sky} is the corresponding sky temperature. The emissivity in Eq. (3.10) was in papers II, III and IV set to 0.9, which is the same value as was used for the other materials, meaning that Eq. (3.9) can be used without adjustments for the differing value of ε. This methodology of measuring q_{sky}, calculating T_{sky} using Eq. (3.10) and thereafter calculating the net radiation using Eq. (3.9) was used in papers II, III and IV.

$$T_{sky} = \sqrt[4]{q_{sky}/(\sigma\varepsilon)} \tag{3.10}$$

There are however methods for estimating q_{sky} without measuring radiation directly, which were not used in this study. When the sky is clear, there is generally a net outflow of heat energy from surfaces on earth. The magnitude of the outflow depends on e.g. the air temperature. This was shown by Idso and Jacksson (1969), who formulated the incoming long wave radiative flux as a function of the air temperature as shown in Eq. (3.11). Combining Eq. (3.10) with Eq. (3.11), a mathematical relation between the air temperature and sky temperature can be determined for times when the sky is clear, as illustrated in Fig. 3.4.

$$q_{sky} = \sigma T_{air}^4 \left(1 - 0{,}261 e^{-7.77*10^{-4}(273-T_{air})^2}\right) \tag{3.11}$$

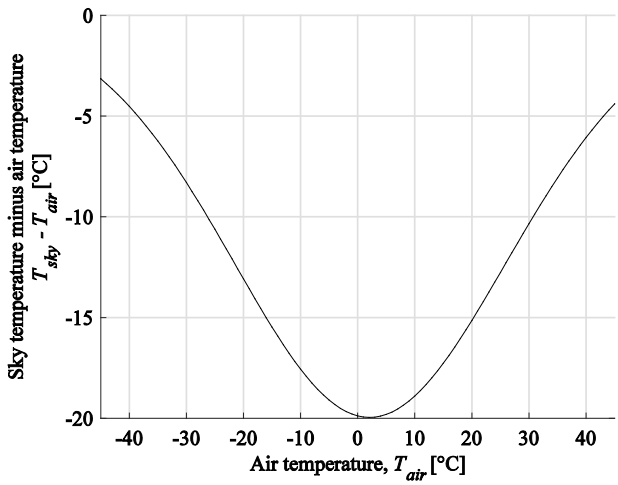

Fig. 3.4. Difference between air and sky temperature as a function of the air temperature, based on relation by Idso and Jacksson (1969).

The model for incoming long wave radiative flux was developed further by Swinbank (1963), who included a dependency of relative humidity. Later models by e.g. Goforth et al. (2002) also included the effect of cloud cover. According to the model, the clouds

increase the incoming long-wave radiation. The reason for this is that the surface temperature of the clouds is generally higher when they are closer to the ground.

These relations can be used to calculate long-wave radiation from air temperature, and if the rate of cloud cover is known, the long wave radiation can be estimated in a simplified way. This methodology was evaluated for use in thermal simulations in portal frame bridges in Larsson Ivanov and Gottsäter (2019), and was shown to give realistic median and extreme values. Therefore, this methodology for estimating long-wave radiation can be used to circumvent the problem of only having a few locations where long wave radiation is measured.

Besides the heat transfer, the temperature of an object is affected by its specific heat capacity. The specific heat capacity, given in [J/(kg·K)], describes the energy required to increase the temperature of an object with a certain mass with a certain number of degrees. If the energy required to heat a certain volume of the material is of interest, the density of the material, in [kg/m^3], must also be considered (Incropera et al., 2007).

Concrete density is usually in the range of 2300–2400 kg/m^3, depending on the porosity, the moisture content and the density of the cement and aggregate. The specific heat capacity depends on the moisture content, water-cement ratio and temperature, and is in the range of 800–1000 J/(kg·K) (Ljungkrantz et al., 1994). For asphalt, density values in the range of 2100–2240 kg/m^3 and values for specific heat capacity in the range of 840–920 J/(kg·K) have been used in previous research listed by Larsson (2012). These values were used in papers II, III, and IV. For soil, the density and specific heat capacity can vary significantly, but density values in the range from 1350 kg/m^3 (dry sand, porosity of 0.5) to 2025 kg/m^3 (dry sand, porosity of 0.25) and specific heat capacity values in the range from 756 J/(kg·K) (dry sand, porosity of 0.5) to 1600 J/(kg·K) (water saturated clay) were used in papers II, III, and IV. The values chosen are based on (Sundberg, 1991).

3.2.2 Heat transfer in portal frame bridges

The most significant climate parameters affecting the temperature in portal frame bridges are air temperature, wind speed, soil temperature, solar radiation and long-wave radiation from the sky. These climate parameters are illustrated in Fig. 3.5. The air temperature and wind speed cause convection along the surfaces facing air. The temperature in the top parts of the bridge, i.e. the bridge deck and abutment, are strongly affected by the air temperature. The temperature in these parts will follow the seasonal variations in air temperature.

The short-term influence of the air temperature depends on the convection, i.e. the wind speed along the bridge surfaces. As the bridge surfaces are facing different directions, and as the bridge structure itself affects the air flow, the exact wind movements along the surfaces are complex and hard to predict. This makes it difficult

to determine the convection along the bridge surfaces correctly at a certain point in time, but reasonable estimations of the structural temperature were obtained from applying the wind speed measured at a weather station close to the bridge on all surfaces facing air, as was shown in paper III.

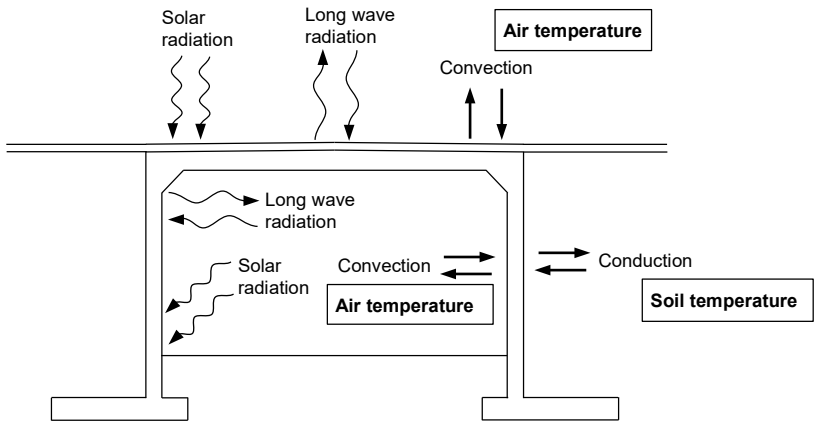

Fig. 3.5. Climate parameters affecting the temperature of portal frame bridges.

The soil temperature is on the other hand more constant over the year. Hillel (2004) illustrated the temperature variation with depth below the soil surface for different seasons, as shown in Fig. 3.6, which clearly shows that a few meters below the ground surface, the seasonal variations in temperature are negligible. Therefore, the temperature of the foundation generally differs more from the air temperature than the temperature in the other parts do. For this reason, the temperature in the foundation is likely to differ more from the temperature in the abutment in areas where the seasonal temperature variations are large, as was shown in paper IV. The constant temperature over the year a few meters below the ground surface was also used to motivate the boundary condition used in the simulations used in papers II, III and IV.

Solar radiation generally increases the temperature of the top surface of the bridge the most, as the top surfaces of bridge decks are often not shaded by other objects. The rest of the bridges are often shaded by the bridge structure itself. The solar radiation has a larger influence on the structural temperature during summer than during the rest of the year.

Long wave radiation from the sky also affects the top of the bridge deck significantly. As long wave radiation is dependent on the temperature of the opposing surfaces as shown in Eq. (3.9), and as the surfaces below the bridge deck which are facing each other can be assumed to have similar temperatures, long wave radiation between these surfaces was neglected in papers III and IV.

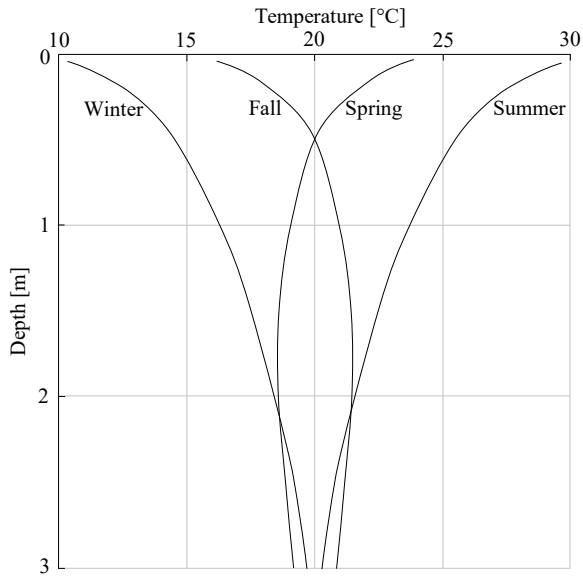

Fig. 3.6. Temperature variation with soil depth in frost-free regions. Figure after Hillel (2004).

There are also other weather related phenomena which can have an impact on the structural temperature of portal frame bridges, but which were not considered in papers II, III and IV. This includes rain, which can either cool or heat the surface layer of the structure, and snow and ice, which changes the color and thus also the absorptivity and emissivity of the surface layer and can also insulate the surface. The material properties of the soil may also vary over time and space within the modeling area. Another effect which was not considered in this study is freezing of the materials, which affects the thermal conductivity and also leads to a release of heat energy. The same amount of energy is required for thawing. However, the verification of the simulation model in paper III showed that the model used had an acceptable margin of error.

3.2.3 Thermal actions in Eurocode

Thermal actions for bridges are presented in CEN (2003), which prescribes various types of temperature distributions to consider in design. These are uniform high and low temperatures, temperature gradients over bridge decks, and temperature differences between main structural elements. There are also some other types of thermal actions mentioned, such as horizontal gradients in bridge decks and temperature differences

between wall faces (possibly applied to abutments), but these are generally not considered in design of portal frame bridges in Sweden.

The uniform high and low temperatures are compared with the temperature at casting, often assumed to be 10°C, in order to calculate the desired movements. The temperature values to consider are specified in isotherm maps. In Sweden, tables with values for each municipally have also been developed. The value is then modified based on the bridge type, e.g. values for bridges with concrete decks are less extreme than values for bridges with steel or composite decks.

The load value for temperature gradients over bridge decks is dependent on the bridge type and surfacing, as well as whether the top or the bottom side is warmest. The value is however not dependent on the bridge location. A linear or multi-linear temperature variation over the cross-sectional height can be assumed, and the load case should be combined with the uniform high and low temperatures in different combinations.

The load case for temperature differences between structural parts is defined in section 6.1.6 of CEN (2003), and is quoted in full below:

> *"(1) In structures where differences in the uniform temperature component between different element types may cause adverse load effects, these effects should be taken into account.*
>
> *NOTE: The National annex may give values for the differences in the uniform temperature component. Recommended values are:*
>
> - *15°C between main structural elements (e.g. tie and arch); and*
> - *10°C and 20°C for light and dark colour respectively between suspension/stay cables and deck (or tower).*
>
> *(2) These effects should be considered in addition to the effects resulting from a uniform temperature component in all elements, determined from 6.1.3."*

The 15°C temperature difference between "main structural elements" has in Sweden been interpreted as to be applied for structural parts in any bridge type, e.g. portal frame bridges. In many other countries, the load case has instead been interpreted as focusing only on the structural parts mentioned in the definition, and is thus not applied for e.g. portal frame bridges. For this reason, the present study has been of most interest in Sweden, and focus has been on Swedish conditions when developing a more detailed description of the load case, adapted for portal frame bridges.

In design of portal frame bridges in Sweden, the temperature differences between bridge deck and abutment, and between abutment and foundation, are often considered simultaneously. A common methodology is to apply a vertical temperature gradient over the abutment height, so that the temperature in the top of the abutment equals

the temperature in the bridge deck, while the temperature in the bottom of the abutment equals the temperature in the foundation. A more conservative interpretation of the load case is to assume a uniform temperature in each structural part. These interpretations can thus result in temperature distributions as shown in Fig. 3.7, of which Fig. 3.7 (a) and (b) or Fig. 3.7 (c) and (d) are chosen to be used in design.

Furthermore, the 15°C temperature difference has by some bridge designers been interpreted as the quasi-permanent value to be used in design situations, while others have interpreted the value as a characteristic load value. The latter interpretation of the load case implies that for crack width limitation calculations, which are performed using quasi-permanent load values, the temperature differences shown in Fig. 3.7 should be multiplied with the ψ_2-factor for thermal actions, i.e. 0.5 (see section 2.1.).

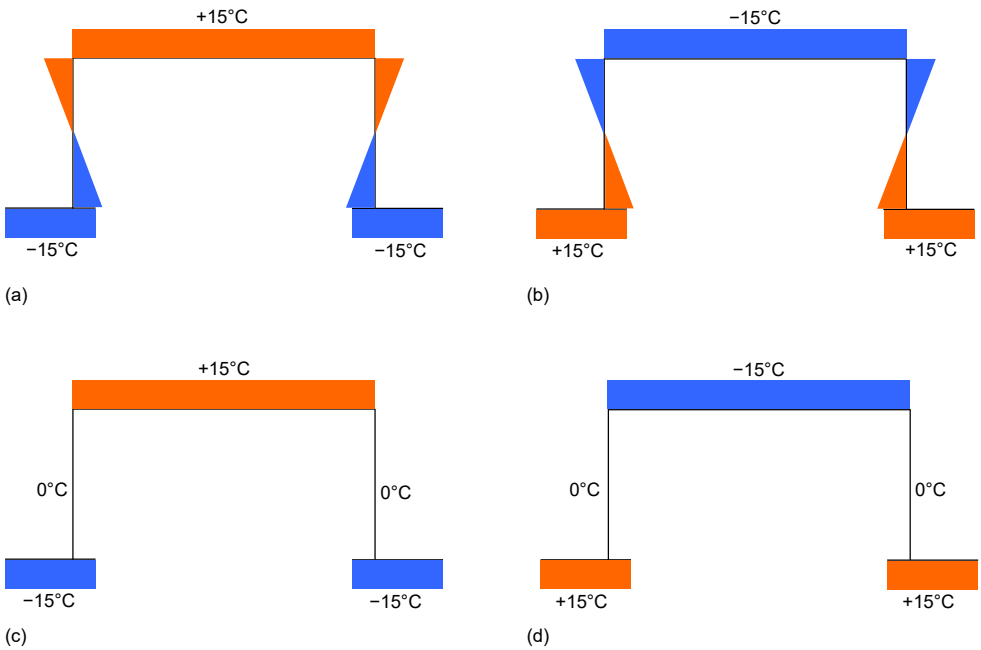

Fig. 3.7. Thermal load case in CEN (2003) section 6.1.6 applied to portal frame bridges, with a gradient over the abutment height (a) and (b), uniform temperature in the structural parts (c) and (d), a warmer bridge deck than foundation (a) and (c), and a colder bridge deck than foundation, (b) and (d).

The background document to the present Eurocode document regarding thermal actions (CEN, 1996) did not clearly motivate the choice of the 15°C load value. However, it was stated that in the previous German code, DIN 1072, a 5°C temperature difference was prescribed between structural parts of concrete, and a 15°C difference was prescribed if one or both parts were constituted of other materials. The previous Swedish code, Bro 2004 (Vägverket, 2004), prescribed a 10°C short-term temperature difference between structural parts, but no long-term temperature

difference. The fact that the load value was a short-term load means that it was not considered in crack width limitation, as crack width limitation is calculated using quasi-permanent loads. This implies that the present load value used in crack width limitation today is high from a historical perspective.

3.2.4 Suggested load cases based on the present study

The present study includes an initial investigation of thermal actions in portal frame bridges, (paper II), a verification of the use of a temperature simulation model for portal frame bridge cross sections (paper III) and the determination of suggested load values for temperature differences between structural parts in portal frame bridges (paper IV). The most important conclusions of the papers are listed below:

Conclusions from paper II:

- It is reasonable to assign different temperatures to the different structural parts, and to consider the transition zones between the structural parts. Considering the transition zones reduces the maximum stress values, and makes the maximum stress appear in slightly different areas than otherwise.
- A 15°C temperature difference, as given in Eurocode, is significantly larger than a realistic quasi-permanent load value for the temperature difference between the bridge deck and abutment of a portal frame bridge. It could however be a reasonable characteristic load value.
- When the largest temperature differences occur, temperature gradients over the cross sections of both bridge deck and abutment are also present.
- When considering the actual temperature distribution at the times for the largest temperature differences between the bridge deck and the abutment, the largest tensile stresses were found at the back side of the abutment, slightly below the corner region.
- The stress distribution can be re-created fairly well by assigning temperature differences between the structural parts, as well as gradients over both the bridge deck and the abutment cross sectional heights. The temperature distribution in the corner area is however hard to describe in a simple way for this situation.

Conclusions from paper III:

- The model for thermal simulations of portal frame bridge cross sections renders realistic results of temperature differences between structural parts.
- When using the model to determine temperature differences at specific points in time, a margin of error of 1.5°C should be added to the result in order not

to underestimate the actual value. However, when determining average values over time, the margin of error was shown to be negligible.

- The temperature difference between the abutment and foundation can be larger than the difference between bridge deck and abutment, and must also be investigated further.

Conclusions from paper IV:

- The largest characteristic load values for the temperature difference between bridge deck and abutment found in the eight data series used were 14.7°C when the bridge deck was the warmer part and 13.7°C when the abutment was the warmer part. Regarding the temperature difference between abutment and foundation, the corresponding values were 18.5°C when the abutment was the warmer part and 26.7°C when the foundation was the warmer part. These values include the 1.5°C margin of error.
- The corresponding quasi permanent values were 4.0°C for when the bridge deck was warmer than the abutment and 1.8°C when the abutment was warmer than the bridge deck. For temperature difference between abutment and foundation, the corresponding values were 6.5°C when the abutment was the warmer part and 5.2°C when the foundation was the warmer part.
- Both characteristic and quasi-permanent load values for temperature differences between abutment and foundation were found to correlate with the difference in average mean air temperature between July and January.
- The difference between the average maximum and minimum air temperature in January correlated with the load values for temperature difference between bridge deck and abutment, both for characteristic and quasi-permanent values, when the bridge deck is colder than the abutment. However, for the case when the bridge deck is warmer than the abutment, no simple correlation with air temperature was found.
- The sizes of the transition zones were found to be independent of the cross-sectional height of the bridge deck and abutment.

Based on the results in the papers, the thermal load case for portal frame bridges which is illustrated in Fig. 3.8 was suggested. The values presented in the figure are based on the values found in paper IV. The temperature is set to 0°C in the abutment, and is then either higher in the bridge deck and lower in the foundation, or lower in the bridge deck and higher in the foundation. To simplify the load cases, the positive and negative temperature values are the same for each structural part and load combination. The values constitute the largest load values found in paper IV, rounded up. The transition zones are also marked in the figure, along which the temperature varies linearly. The length of the transition zone in the frame corner is independent of the bridge geometry,

and the length of the transition zone between abutment and foundation is only dependent of the depth of the foundation below the surface under the bridge.

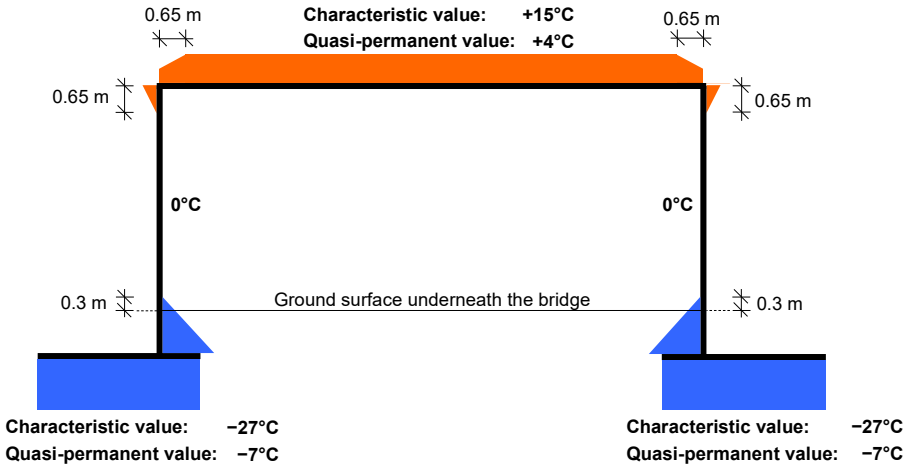

(a)

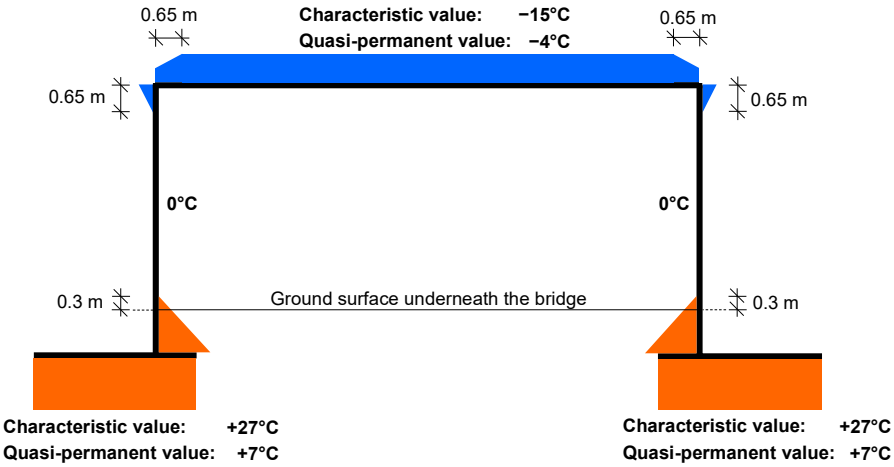

(b)

Fig. 3.8. Proposed thermal loads for the load case describing temperature differences between structural parts. (a) describes the case when the bridge deck is the warmest structural part and (b) describes the case when it is the coldest part. The figure shows the system line of the structure. Linear temperature variations are assigned to the transition zones between the parts with constant temperature.

3.2.5 Discussion regarding the suggested load cases

The suggested thermal load case does not include gradients over the bridge deck and abutment, as was investigated in paper II. The reason for this is that these load effects are already described by other load cases, which can be considered in design.

The largest characteristic temperature difference between bridge deck and abutment when the deck is the warmest structural part was obtained using data from Lund, and the largest corresponding quasi-permanent value was obtained using data from Norrköping. However, all of the other largest temperature differences were obtained with data from Kiruna or Luleå, situated in the north of Sweden. A relation between the load values and aspects of the air temperature variations over the year were found and presented in paper IV, which explains these results. The load values were generally significantly lower in southern coastal locations than in northern locations, which indicates that the load values could be reduced in parts of the country. However, reducing the load values in certain regions requires thermal simulations with weather data from more locations. As of today, the available data is especially limited for solar and long wave radiation. The required data could however be obtained using calculated values for solar and long wave radiation, as investigated in Larsson Ivanov and Gottsäter (2019) and discussed in section 3.2.1.

The suggested load cases apply the temperature difference between the bridge deck and abutment simultaneously with the difference between abutment and foundation. Investigations of the occurrence of extreme values indicate that extreme values of the two temperature differences often coincide, which is illustrated in Fig. 3.9. The figure shows the temperature difference between bridge deck and abutment as well as between abutment and foundation, during a one-year period using weather data from Kiruna. The temperature differences have been normed so that the maximum and minimum values of each temperature difference during the chosen time period corresponds to 1. The norming was done as the largest temperature difference between abutment and foundation was significantly larger than that between bridge deck and abutment. Positive values are defined as when the bridge deck is warmer than the abutment, and when the abutment is warmer than the foundation, respectively. Negative values thus correspond to the bridge deck being colder than the abutment, and the abutment being colder than the foundation, respectively.

The temperature differences could also be considered one at a time, in which case the largest load value from the two analyses for each point in the structural model would be used, although this situation is unlikely to occur according to Fig. 3.9. However, significant differences in the results compared to when the temperature differences are considered simultaneously only occur in bridges which have abutments with large width to height ratios. When the width to height ratio is 5, the difference is e.g. up to 0.5 MPa. For the case when the bridge deck is warm and the foundation is cold, considering the temperature differences separately causes the tensile stresses to increase in the foundation and the bridge deck, and to decrease in the abutment.

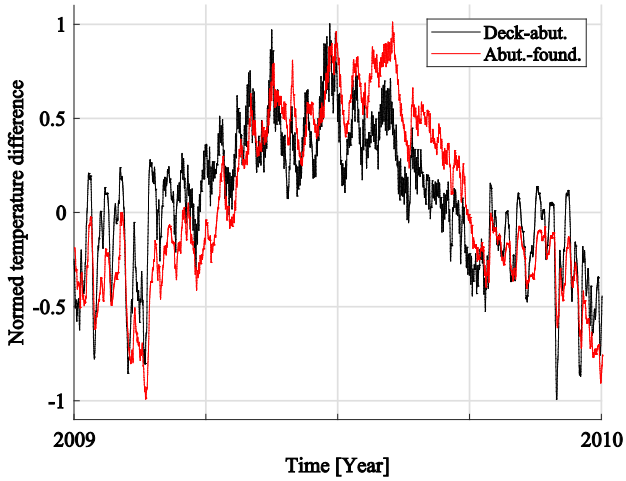

Fig. 3.9. Normed temperature differences between bridge deck and abutment as well as between abutment and foundation, for simulation with data from Kiruna, year 2009.

The transition zones were in paper IV shown not to change significantly in length when the thickness of the bridge deck and abutment was varied. This was also the case when the bridge deck and abutment were assigned different thicknesses, as is shown in Fig. 3.10. The figure shows the temperature along the system line at the time for the largest temperature difference between bridge deck and abutment, which occurred with data from Lund on the 6th of July 1985 for the case when the bridge deck is warmer than the abutment (Fig. 3.10 (a)) and with data from Kiruna on the 8th of January 2016 for the case when the bridge deck is colder than the abutment (Fig. 3.10 (b)). The small figure of a portal frame bridge cross section which is also shown in Fig. 3.10 (a) illustrates the system line and marks points of interest along it. These points are also marked along the horizontal axes of the graphs. The darker areas in the cross section shown are the areas used to determine the temperature in the structural parts, and the lighter areas are the transition zones. Note that the transition zone between abutment and foundation used in the design model, as shown in Fig. 3.8, covers the entire distance from "E" to "G", even though the entire foundation has been used in the determination of the foundation temperature.

Fig. 3.10 also indicates that the temperature difference between bridge deck and abutment increases when the cross-sectional height is smaller in the bridge deck than in the abutment, and that it decreases when the cross-sectional height is larger in the bridge deck. In real portal frame bridges, the cross-sectional height is however generally not smaller in the bridge deck than in the abutment. This means that a realistic worst case scenario is when the cross-sectional heights are equal, which was assumed in the model used for determination of load values. It can also be seen in Fig. 3.10 that the temperature difference between abutment and foundation is larger when the abutment

cross-sectional height is small, which explains why an abutment with a relatively small cross-sectional height was used when load values were determined.

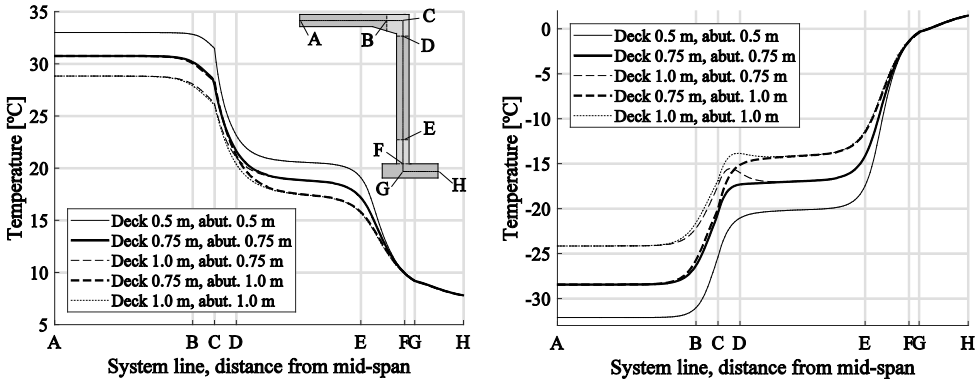

(a) (b)

Fig. 3.10. Temperature along the system line for the cases when the bridge deck is the warmest structural part (a) and the coldest structural part (b). Results are shown for 5 different combinations of bridge deck and abutment thicknesses.

The length of the transition zone in the lower part of the abutment was in Fig. 3.8 defined as the vertical distance from the foundation center of gravity to 0.3 m above the ground surface underneath the bridge. This definition is in Fig. 3.11 shown to be reasonable for a variety of levels of the ground surface under the bridge, i.e. for different depths of the foundation. The figure shows the temperature along the system line the same way as in Fig. 3.10, for different positions of the top end of the transition zone, i.e. the position of "E". The figure legends indicate the lengths of the entire transition zones as defined in Fig. 3.8, i.e. the distance between "E" and "G". The temperature distribution shown was obtained with data from Kiruna on the 11th of June 2011 in Fig. 3.11 (a) and from Kiruna on the 6th of February 2012 in Fig. 3.11 (b). On these occasions, the largest temperature differences between abutment and foundation were found.

It can also be seen in Fig. 3.11 that the temperature difference between abutment and foundation increases when the depth of the foundation increases. Also, the temperature reaches an extreme value at the end of the abutment, denoted "H". Although the distance between "E" and "G" was 1.6 m in the simulations used to determine the thermal load values presented in Fig. 3.8 and a longer distance would result in a larger load value, the presented load values are considered to be sufficiently conservative. One reason for this is that the major parts of the foundations are directed away from the bridge in horizontal direction, where the temperatures are more extreme, i.e. to the right of "G" in the illustration in Fig. 3.11 (a).

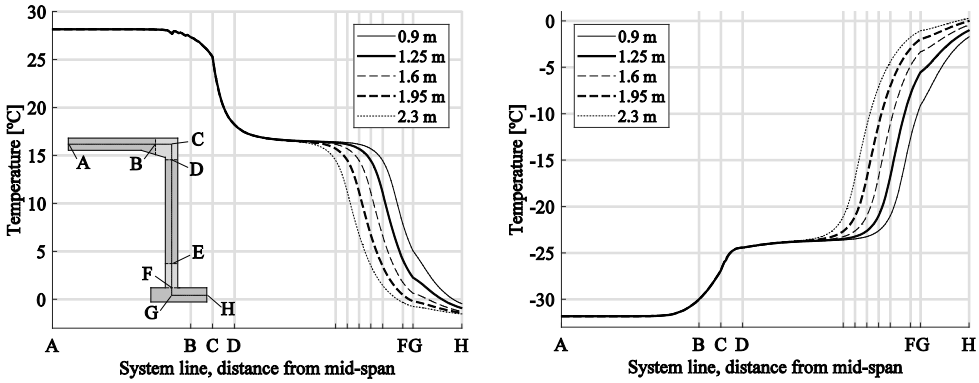

Fig. 3.11. Temperature along the system line according to different levels of the ground below the bridge, which affects the position of "E". The legend shows the length of the transition zone between the two parts in the different simulations, i.e. the distance "E" to "G".

The influence of the tapering of the frame corner on the temperature along the system line was also investigated. This was done by comparing results from using no tapering with results from one model with a 0.3 m vertical and 1 m horizontal tapering, and another model with a 0.6 m vertical and 2 m horizontal tapering. The comparison is shown in Fig. 3.12, using the same weather data as for Fig. 3.10. The figure shows that the tapering has no influence on the temperature along the system line when the bridge deck is warmer than the abutment, but that it has an influence when the bridge deck is colder than the abutment.

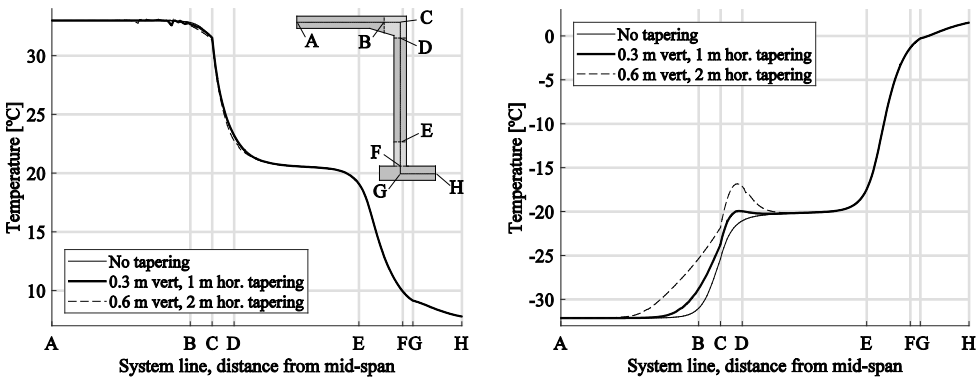

Fig. 3.12. Temperature along the system line for different sizes of the tapering in the frame corner.

The explanation for these different effects of the tapering is that when the bridge deck is significantly warmer than the abutment, solar radiation has a large impact on the

structural temperature. Therefore, heat is thus transmitted from the top of the structure towards the lower parts. As the tapering is neglected when determining the position of the system line, the tapering thus has a negligible effect on the temperature in the frame corner. On the other hand, when the bridge deck is cold, heat is transmitted rather equally from all sides of the structure facing air, in which case a large tapering insulates the frame corner. The influence of the size of the tapering has however been disregarded when determining the lengths of the transition zone in the frame corner in the load cases. As longer transition zones reduce the stresses in the model, disregarding the influence of a large tapering and thus keeping the transition zone short is assumed to be on the safe side.

Taking this information into account, the thermal load cases presented in Fig. 3.8 are expected to correspond to an unfavorable situation, as they were determined with the most unfavorable weather data available, and for a cross-sectional geometry which has been shown to be unfavorable as well. This means that the load cases presented in Fig. 3.8 can be used in design of portal frame bridges of general geometry in a Swedish climate.

3.2.6 Special cases with reduced load values

The load case presented in Fig. 3.8 is developed for a portal frame bridge with the principal geometry as shown in the figure, and can be used for portal frame bridges in general. However, the load case can be considered to be significantly exaggerated for at least two types of portal frame bridges, which have been investigated further within this study. These are bridges with a layer of gravel on the bridge deck of at least 300 mm, and bridges with a single foundation for both abutments, for which the foundation is only covered by a layer of asphalt paving of no more than 200 mm. These two bridge types are illustrated in Fig. 3.13.

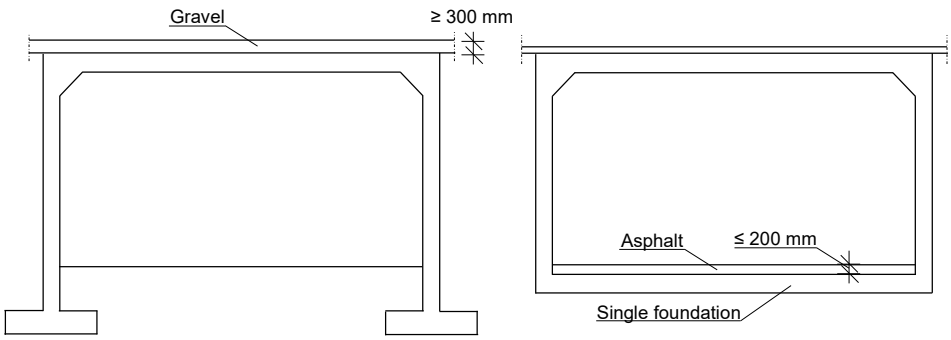

Fig. 3.13. Illustrations of geometries where the special load cases regarding gravel on the bridge deck (a) and single foundation (b) are applicable.

Placing a layer of gravel with a thickness of at least 300 mm on the bridge deck is common for bridges carrying railway traffic.

As the gravel insulates the bridge deck better than the asphalt paving, the temperature differences between bridge deck and abutment can be expected to become smaller in this case. The determination of the load values for this type of bridge was performed using the same model and methodology as in paper IV. The structural model was however modified, with a 300 mm gravel layer placed upon the bridge deck, which was assigned the same material properties as the fill used in paper IV. Also, only weather data from Lund, Kiruna and Luleå was used in the analyses. The resulting load values obtained with each data set is presented in Table 3.1. Based on these values, characteristic temperature differences between the bridge deck and the abutment of 10°C and corresponding quasi-permanent values of 2°C was suggested for this special case.

Table 3.1. Thermal load values in [°C] obtained using the different data series used to simulate temperature for a portal frame bridge with a gravel layer of at least 300 mm on the bridge deck.

Load type	Kiruna 08–17	Luleå 88–97	Lund 84–00
Characteristic value, bridge deck warm	8.0	6.9	7.7
Characteristic value, bridge deck cold	9.2	8.8	6.5
Quasi-permanent value, bridge deck warm	1.9	2.0	1.8
Quasi-permanent value, bridge deck cold	1.3	1.2	0.8

For bridges with a single foundation for both abutments, the temperature difference between abutment and foundation can be reduced. The foundation is generally placed closer to the ground surface under the bridge for this type of structure, and often with only asphalt paving placed on top of it. This motivates the reduction of the temperature difference. The load values for this situation were also determined using the same model as in paper IV, with an adjusted structural model. A relatively thick asphalt layer of 200 mm was placed on the foundation, as a thicker layer will lead to increased temperature differences between the abutment and foundation. Only data from Lund, Luleå and Kiruna were used in the analyses of this special case as well. The resulting load values obtained with each data set is presented in Table 3.2. Based on these values, characteristic temperature differences between the abutment and the foundation of 10°C and corresponding quasi-permanent values of 2°C was suggested for this special case.

In these analyses, it has been assumed that the road surface below the bridge deck is shaded (as it has in all other simulations). If it instead is assumed that solar radiation reaches the surface of the road under the bridge, the temperature difference could be reversed, i.e. the foundation could become warmer than the abutment during the

summer. This has however not been investigated further, and possible tensile stresses resulting from this situation is assumed to be smaller than tensile stresses caused by the suggested load cases.

Table 3.2. Thermal load values in [°C] obtained using the different data series used to simulate temperature for a portal frame bridge with a single foundation.

Load type	Kiruna 08–17	Luleå 88–97	Lund 84–00
Characteristic value, bridge deck warm	8.4	7.3	7.1
Characteristic value, bridge deck cold	9.7	9.9	8.3
Quasi-permanent value, bridge deck warm	1.6	1.7	1.2
Quasi-permanent value, bridge deck cold	1.5	1.5	0.9

The suggested load values to be used in design of these portal frame bridges are summarized in Table 3.3, which also shows the load values for the general case. For bridges fulfilling both conditions of the special load cases, the lower load values can be used for both temperature differences simultaneously, i.e. the load case can consist of 10°C characteristic and a 2°C quasi-permanent temperature differences only.

Table 3.3. Temperature differences suggested for the general load case and the two special cases investigated.

	General load case	≥300 mm gravel on bridge deck	Single foundation, ≤200 mm asphalt on foundation
Characteristic temperature difference, bridge deck–abutment	±15°C	±10°C	±15°C
Quasi-permanent temperature difference, bridge deck–abutment	±4°C	±2°C	±4°C
Characteristic temperature difference, abutment–foundation	±27°C	±27°C	±10°C
Quasi-permanent temperature difference, abutment–foundation	±7°C	±7°C	±2°C

3.3 Shrinkage in portal frame bridges

Shrinkage is a process of volume loss in concrete due to either the concrete drying out after the curing, called drying out shrinkage, or the chemical binding of water to the cement paste during the hardening phase, called autogenous shrinkage. The autogenous shrinkage occurs during curing, and its magnitude depends on the concrete strength and cement type (fib, 2013). The drying out shrinkage on the other hand develops slowly, as the concrete slowly adapts its relative humidity (RH) to the surrounding environment after being water saturated during curing.

The rate of drying out shrinkage is often discussed in terms of reference shrinkage, i.e. shrinkage occurring in concrete in a standardized environment with regards to age at shrinkage initiation, RH and temperature (Ljungkrantz et al., 1994). The reference shrinkage depends on the water ratio in the concrete, which means that the shrinkage varies both with the water-cement ratio and the volume rate of cement and filler in the concrete (Bureau of Reclamation, 1942).

In Eurocode (CEN, 2005a), the final value of the drying out shrinkage is determined by the RH of the surrounding environment, the concrete strength class and the cement type. The so called notional size is also considered when determining the final shrinkage value, which corresponds to two times the cross sectional area divided with the perimeter of the cross section exposed to drying. A large notional size reduces the calculated final shrinkage value, as thick structures can take many years to dry out completely.

When shrinkage occurs, the cement volume is reduced, while the aggregate does not desire to change its volume. This means that even unrestrained shrinkage will cause stresses in concrete, as the cement paste will be in tension while the aggregate will be in compression (Ljungkrantz et al., 1994). In this study, the concrete is however only considered as a homogenous material, and the material components are not considered separately from each other.

Since shrinkage only occurs in concrete and not in the reinforcement, the reinforcement will counteract the shrinkage, which causes stresses in the structure. The actual change of e.g. the length of a structural member will thereby not only depend on the magnitude of shrinkage, but also on the stiffness relationship between the concrete and the reinforcement.

In section 4.5 and in paper VI, a difference in shrinkage of 10^{-4} between the foundations and the rest of the portal frame bridge was included in the analyses. This shall correspond to shrinkage resulting from casting the bridge in two stages, as discussed in section 2. When calculating shrinkage using Eurocode (CEN, 2005a), the value 10^{-4} corresponds to the sum of the autogenous shrinkage and drying out shrinkage developing in the foundations during 250 days, assuming concrete quality C40, 80% RH and the foundations drying out from the top edge only. The chosen value for the shrinkage difference is therefore considered to be larger than what is expected in most practical cases, and thus unlikely to underestimate the load effect.

4 Cracking in portal frame bridges

4.1 The problem with cracking in concrete bridges

The need to limit cracking by the use of reinforcement arises as concrete is a brittle material with often more than ten times higher strength in compression than in tension. When the tensile stresses in concrete surpasses the stress capacity, usually at a strain of about 10^{-4}, cracking occurs (Ljungkrantz et al., 1994). The cracks risk exposing the reinforcement to corrosive agents, such as chlorides. It also enables carbonation along the crack, which reduces the pH-value of the concrete. A lowered pH-value in turn enables corrosion to take place (Zhou et al., 2015) which can reduce the durability of the structure significantly. Several other negative effects can also be found, such as increased water permeability and impaired aesthetic appearance.

Cracking in concrete can be caused by e.g. restraint effects, external loads or chemical degradation, at any stage of the structural life time. Some examples of different types of cracks appearing at different stages of the life time are plastic settlement cracks appearing only a few minutes after casting, plastic shrinkage cracks appearing after a few hours, surface crazing and cracking due to thermal actions occurring after a few days of curing, and long term drying shrinkage cracks appearing after several weeks or months. Cracking caused by thermal actions due to ambient climate or external loading can occur at any time after the curing phase (The Concrete Society, 1992). Causes of cracking in concrete structures is discussed further in e.g. The Concrete Society (1992), Halvorsen (1993), Ljungkrantz et al. (1994), ACI Committee 224 (1998), ACI Committee 224 (2001) and Frosch et al. (2003).

For bridges, which are often exposed to moisture, freeze-thaw cycles and de-icing agents, crack widths are to be limited in order to limit the deterioration of the structure. The crack width has a clear impact on the speed of the corrosion process in a short term perspective, with wider cracks leading to the corrosion process being faster. The influence of crack widths on the speed of the corrosion process in a long term perspective is however debated, where some studies indicate that crack widths are still relevant to the magnitude of long term corrosion, while other studies indicate that the long-term effect is independent of the width of the cracks (Beeby, 1983), (Otieno et al., 2010), (François et al., 2012). A further investigation of the rationale of securing durability by limiting crack widths is however beyond the scope of this study.

To the author's knowledge, no study of cracking due to restraint effects in portal frame bridges, which can be related to differences in temperature or shrinkage between structural parts, has previously been performed. Several studies have however been performed on cracking due to restraint in other types of bridges, e.g. by Schmitt and Darwin (1995), Portland Cement Association (1970), Krauss and Rogallla (1996), Poppe (1981) and Frosch et al. (2003). One of the findings in these studies is that girder bridges, which are common in the US, are prone to cracking shortly after construction, and that this relates to shrinkage and thermal actions. This is discussed more in detail by Brown et al. (2001). One solution to the problem is presented by Saadeghvaziri and Hadidi (2005), who suggests that the stiffness of the girders must be reduced in relation to the stiffness of the bridge deck.

In Sweden, the Swedish Transport Administration is responsible for the maintenance of most of the bridges. The agency uses a database called BaTMan, acronym for "Bridge and Tunnel Management" (Trafikverket, 2018), in which information about the bridges is stored. The database contains e.g. information regarding past and present damages in bridges. A smaller study performed within this project investigated the occurrence of different types of damage on Swedish portal frame bridges. The most common damage types (noted in over 1000 structural parts) in portal frame bridges at the time of the study (February 2015) are listed in Table 4.1. The labeling of the damage is not completely standardized, as it can be hard to define e.g. crack types. The study did not consider the severity of the damages, therefore it is unknown how many of the reported damages that were to be mitigated and how many that were considered acceptable.

Table 4.1. The most common damage types in Swedish portal frame bridges based on data from BaTMan, February 2015.

Damage type	No of affected structural parts
Cracking due to tension	6330
Spalling	3250
Weathering	2717
Corrosion	1674
Cracking	1441
Crushing	1124

Table 4.1. shows that cracking is the most common damage type in portal frame bridges in Sweden. The cause of the damage is also stated in the database, and a summary of the given causes of cracking in the portal frame bridges is shown in Table 4.2. The cause of cracking is however often difficult to determine, and is in reality often a combination of effects. Also, the labeling is not standardized in this case either. Therefore, some of the crack causes given in the table are vaguely formulated. The table does however show that shrinkage is considered to be the most common cause of cracking, while thermal actions are considered to cause only a small minority of the cracks. It can therefore be stated that restraint effects are considered to be the main

cause of cracking in portal frame bridges. As cracks due to shrinkage and thermal actions can be hard to differ for each other, and as these effects often occur simultaneously, further investigations of cracking due to both thermal actions and shrinkage is motivated.

Table 4.2. The most common causes for cracking in Swedish portal frame bridges based on data from BaTMan, February 2015. Crack causes have been listed for the damage types "Cracking due to tension", "Cracking" and "Cracking due to bending".

Cause of cracking	No of affected structural parts
Shrinkage	2963
Load/action – type not stated*	1789
Undetermined cause	1699
Construction error	850
Environmental effect	276
Curing	202
Thermal action	162
Traffic load	123
Alkali-silica reaction	82
Frost damage	76
Chemical attack	70

* In the damage reports which were written in Swedish, the word "belastning" was used.

4.2 Cracking in reinforced concrete

In uncracked reinforced concrete, the strain in a reinforcement bar and the concrete surrounding it is equal. At this stage, the difference in stress between concrete and reinforcement depends on the difference in Young's modulus. For short-term loads, the Young's modulus of the reinforcement is about six times larger than the Young's modulus of the concrete. Therefore, the stresses in the reinforcement will be about six times larger than in the concrete. As the reinforcement often only constitutes a small part of the cross sectional area (usually below 2%), it will not significantly increase the force needed to cause cracking. However, after cracking has occurred, the reinforcement carries all tensile stresses in the cracked sections. This is why reinforcement does not prevent cracking from occurring, but enables the structure to carry loads after cracking has occurred. If sufficient reinforcement is placed in the structure, the load can be increased substantially after cracking (Ljungkrantz et al., 1994). In many applications, cracking in reinforced concrete is seen as a necessary feature, in order for the structure to carry loads efficiently.

The reinforcement bar and the concrete surrounding it strive to have equal strain. However, as the reinforcement bar carries all stresses over cracked sections, the strain in the bar is substantial in this section, while the concrete strain equals zero. Therefore, tensile stress is transferred from the reinforcement to the concrete along a certain

distance beside the crack, until the strain is equal in the materials. This distance is called the transmission length, and the stresses between the reinforcement and concrete along it are called bond stresses (Engström, 2014).

Fig. 4.1 illustrates a reinforced concrete bar subjected to a tensile force F, which has caused the formation of a crack in the bar. The stress in the concrete (σ_c) and the reinforcement (σ_s) are also illustrated in the figure, as well as the bond stresses along the bar (τ_b). Within the transmission length (l_t) no new crack can form, as the concrete stress cannot reach the strength value that close to an already cracked section. This limits the number of cracks that can form in the bar to what is called a stabilized crack pattern, and implies that the distance between cracks will be between l_t and $2l_t$ when the stabilized crack pattern is reached (Engström, 2014).

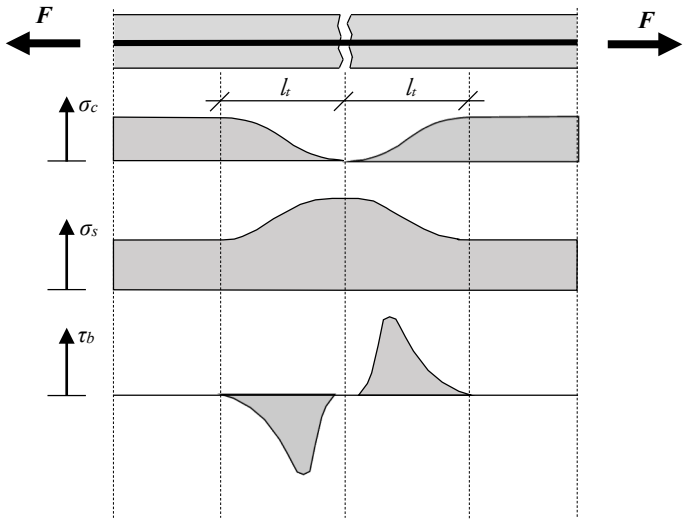

Fig. 4.1. Principal variation of stresses in concrete and reinforcement as well as bond stresses along a reinforced bar with a crack, subjected to tension. Figure after Engström (2014).

The transmission length can be derived from the bond-slip relation between the two materials. This bond is for normal reinforcement mostly caused by the ribs on the reinforcement bars, causing a mechanical connection between the materials (Ljungkrantz et al., 1994). The bond stress in a given cross section depends on, among other factors, the slip between concrete and reinforcement in the specific section. It therefore varies along the transmission length, which is illustrated in Fig. 4.1. The principal variation in bond stress as a function of slip is shown in Fig. 4.2.

Jaccoud (1997) presented a mathematical expression for the ascending part of the curve in Fig. 4.2, which is given in Eq. (4.1) and was used in papers V and VI. The formulation was evaluated by comparing calculated crack widths with results from full-scale tests performed by Jaccoud (1987) and Farra (1995). In the equation, τ_b is the

bond stress in [Pa], f_{cm} is the concrete compressive strength in [Pa] and s is the slip in [mm]. The ascending part of the function is in the expression assumed to end at slip values of 1 mm. As crack widths in serviceability limit state should be significantly smaller than 2 times 1 mm (the same slip occurring on both sides of the crack), the descending part of the curve is not investigated further in this study, although a rough estimation of this part was implemented in the bond-slip formulation used in papers V and VI.

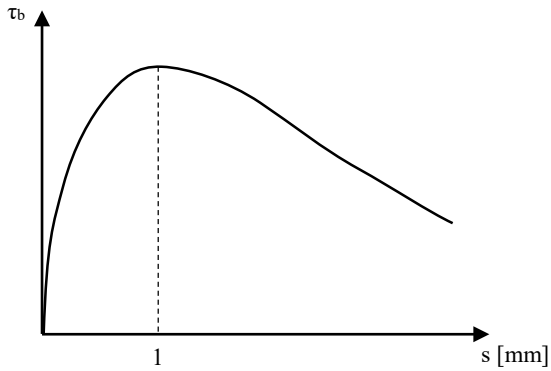

Fig. 4.2. Bond stress as a function of slip for short term loading of a reinforced concrete bar. Figure after Jaccoud et al. (1996).

$$\tau_b = 0.22 f_{cm} s^{0.21} \tag{4.1}$$

Several other mathematical expressions for the ascending part of the bond slip curve corresponding to Eq. (4.1) have been suggested, e.g. by Farra (1995) and Model Code 2010 (fib, 2013). Soroushian and Choi (1989) also suggested an expression, which assumed that the ultimate bond stress depends not only on the compressive strength of the concrete, but also on the reinforcement diameter.

Using Eq. (4.1), Jaccoud (1997) derived an expression for the mean crack width, w_m, and the transmission length, l_t. The expressions given in Jaccoud (1997) were reformulated by Engström (2014) into the forms shown in Eqs. (4.2–4.3).

$$w_m = 0.420 \left(\frac{\varphi \sigma_s^2}{0.22 f_{cm} E_s \left(1 + \frac{E_S \ A_S}{E_c A_{eff}} \right)} \right)^{0.826} + \frac{\sigma_s}{E_s} \cdot 4\varphi \tag{4.2}$$

$$l_t = 0.443 \frac{\varphi \sigma_s}{0.22 f_{cm} \left(w_m - \frac{\sigma_s}{E_s} \cdot 4\varphi \right)^{0.21} \left(1 + \frac{E_S \ A_S}{E_c A_{eff}} \right)} + 2\varphi \tag{4.3}$$

Eqs. (4.2–4.3) show that the mean crack width and transmission length can be expressed as functions of the reinforcement diameter, φ, the reinforcement stress in the cracked section, σ_s, the mean concrete compressive strength, f_{cm}, the Young's modulus of reinforcement and concrete, E_s and E_c, respectively, the reinforcement area, A_s and the effective concrete area of the cross section, A_{eff}. SI-units are used, except for φ, l_t and w_m, which are in [mm].

In crack width limitation, the characteristic crack width, w_k, is used, and not the mean crack width, w_m. In order to calculate w_k from w_m, CEB (1985) gives the expression shown in Eq. (4.4), which is given for restraint situations. In non-restraint situations, the factor differing the values equals 1.7, but for restraint cases, the value is reduced. The reasons given for the reduction are that restraint cracks generally have smaller variations in width, and that the cracking reduces the restraint effects.

$$w_k = 1.3 w_m \tag{4.4}$$

4.3 Cracking due to restraint effects

4.3.1 End-restrained reinforced concrete bars

It was shown in Eq. (3.1) that the magnitude of the restraint stress depends on the restrained strain and the Young's modulus of the material. For end-restrained bars, the restraint force thus depends on the restrained strain multiplied by the cross-sectional stiffness EA, as shown in Eq. (4.5). In the equation, F is the restraint force, ε_R is the restrained strain, A is the cross sectional area and E is Young's modulus (Engström, 2014).

$$F = \varepsilon_R E A \tag{4.5}$$

In cracked sections, the stiffness EA is only constituted by the reinforcement. This corresponds to a significantly lower stiffness than in uncracked sections. Cracking will thereby reduce the stiffness of a structure and thus also reduce the restraint forces. However, Eq. (4.5) can only be used directly to calculate restraint forces if ε_R, E and A are constant along the element, which is not the case if cracks have formed.

The effect of cracking on the restraint force in end-restrained bars is illustrated in Fig. 4.3 (a). In the figure, the end restrained reinforced bar is subjected to a decrease in temperature, ΔT, which causes restraint stresses. Due to force compatibility, the tensile force F must be constant along the entire bar. The bar can therefore be considered as a system of springs connected in a series, for which the total elongation corresponds to the restrained elongation. The force caused by the elongation thereby corresponds to

the restraint force. Before cracking occurs, the stiffness k is equal in all the springs, assuming they are corresponding to parts of the reinforced bar with equal lengths. The strain ε is thereby also equal in the springs.

In the spring model in Fig. 4.3, the first crack that forms causes a reduction of the stiffness of the spring in which the crack is situated. If the length of this spring corresponds to about half the total transmission length on both sides of the crack, the spring will now have a stiffness corresponding to the reinforcement bar only, while the stiffness of the other springs is unchanged. The formation of the crack does not affect the total elongation of the bar, as the total desired elongation due to the thermal action is unaffected by the cracking. However, the force in the element is reduced, as the stiffness of one of the springs is reduced. On the other hand, the strain, which was equal in the springs before cracking, is now increased in the weaker spring, and reduced in the other springs. This development is illustrated in Fig. 4.3 (b). The model presented here is a simplified version of the model used in Eriksson and Fritzson (2014).

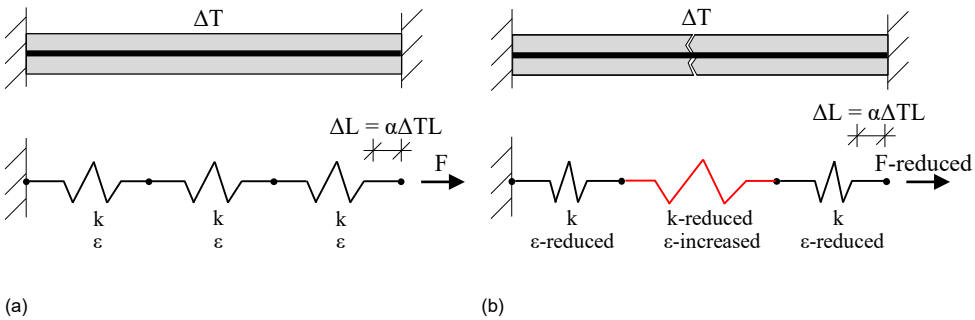

Fig. 4.3. Illustration of a bar which is uncracked (a) or has one crack (b) with spring models of the bars shown below.

As non-restraint forces are unaffected by the structural stiffness, the cracking phase will look different depending on whether restraint or non-restraint forces are acting on the structure. In order to illustrate this difference, another example of a reinforced concrete bar is shown, see Fig. 4.4 (a). If the bar is subjected to a continuously increasing external load, the bar will go from uncracked to a stabilized crack pattern over a very small increase in loading, due to the small variations in concrete material properties along it, see Fig. 4.4 (b). The elongation of the bar, ΔL, can be expressed as in Eq. (4.6), which shows ΔL as a function of the force F, the length of the bar, L, and the average stiffness AE. As can be seen in the equation, the elongation is drastically increased for every new crack formed, as the stiffness of the bar is reduced.

$$\Delta L = FL/(AE) \tag{4.6}$$

If instead the elongation is continuously increased, the load – elongation relation will look different, as shown in Fig. 4.4 (c). When the stiffness decreases in this case due to

the formation of a crack, the force must also decrease in order for the elongation to remain unchanged. As the elongation continues to increase, a new crack will form each time the tensile strength of the concrete is reached.

The most important differences between the two cases illustrated in Fig. 4.4 (b) and (c) are that in the restrained case, cracking reduces the stresses in the specimen, and that the development from one crack to the stabilized crack stage requires a significant increase in restraint. This difference in behavior is discussed in e.g. Jokela (1984), Ghali and Favre (1994), Elbadry and Ghali (1995), Balázs (2013) and Engström (2014).

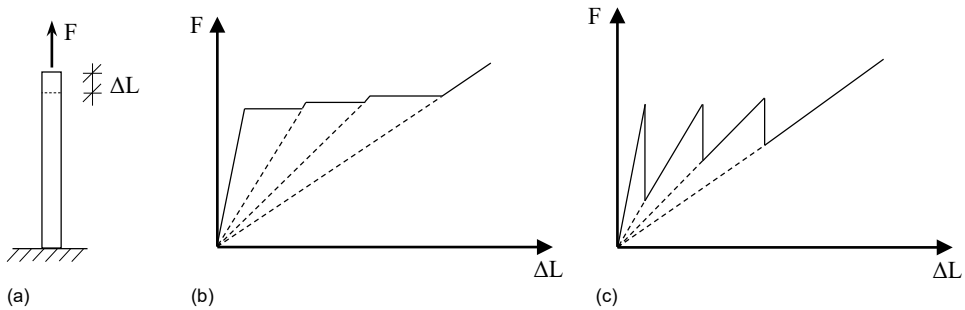

Fig. 4.4. Comparison of load-deformation diagram of a reinforced concrete bar (a) subjected to a continuously increasing external load (b) or a continuously increasing elongation (c), corresponding to increasing restrained deformations. Figure after Ghali and Favre (1994), Elbadry and Ghali (1995), Balázs (2013) and Engström (2014).

The conclusion that a significant increase in restraint is required to reach the stabilized crack pattern after the first crack has formed means that it can normally not be assumed that a stabilized crack pattern is reached when restraint stresses are dominating. This implies that the stiffness, and therefore also the restraint stresses of the specimen, are hard to predict. Fig. 4.5 shows the same load-elongation pattern as Fig. 4.4 (c), but with the stiffness of the uncracked stage (stage I) and the stabilized crack stage (stage II) marked. The stage I stiffness is denoted EA_I, and the stage II stiffness is denoted EA_{II}.

Fig. 4.5 illustrates that if the stabilized crack pattern is not reached, the entire crack development process must be known in order to estimate the number of cracks and thereby the stiffness and stresses in the model. Using the stage I stiffness would in this case overestimate the stresses, while using the stage II stiffness would underestimate the stresses. This is illustrated by the forces F_I and F_{II} in Fig. 4.5, which are estimations of the restraint force F_R at the restrained elongation ΔL_R, using stage I and II stiffnesses, respectively. The stage II stiffness can be estimated beforehand by considering the distance between cracks at the stabilized cracking stage. As the expressions for crack width in Eurocode 2-1-1 (Eqs. 2.1–2.3) do not describe the reduction of restraint stresses due to cracking, there is no consideration of this stress reduction in the common design method. This implies that if the effects of cracking are not considered in another way during design, the resulting stresses from the calculations will correspond to F_I in Fig. 4.5, and thus risk being significantly exaggerated.

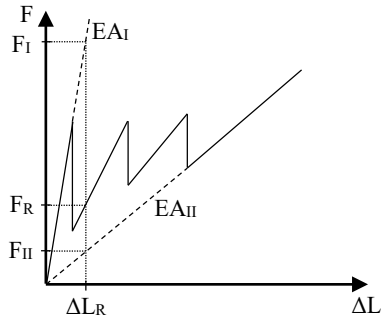

Fig. 4.5. Load-deformation diagram of an end-restrained bar subjected to restraint effects. A restrained elongation ΔL_R causes the restraint force F_R. Estimating F_R by using the state I stiffness EA_I or by using state II stiffness EA_{II} gives the inaccurate results F_I or F_{II} respectively.

In order to illustrate how crack widths and the number of cracks in an end-restrained reinforced concrete bar can be calculated, Example 1 is shown. The calculations in the example are made using Eq. (4.2) for a uniform temperature decrease in the bar, and are based on expressions from Engström (2014) and similar calculations in Nesset and Skoglund (2007). Calculations are also performed without including the stress reduction due to restraint, for comparison.

Example 1: Calculation of crack width in an end restrained reinforced concrete bar

The bar is fully restrained from any horizontal movements, and subjected to a temperature decrease of $\Delta T = -10°C$. Material and cross sectional data is given below.

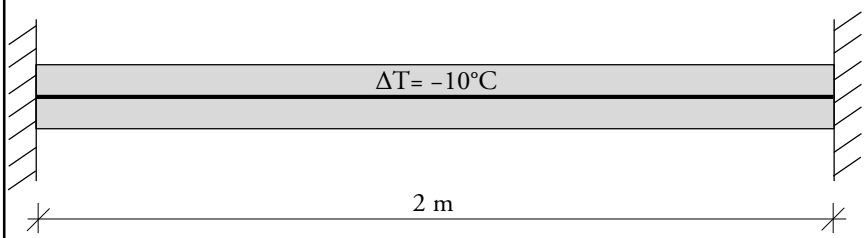

Parameter	Notation	Value	Unit
Concrete tensile strength	f_{ct}	2.2	MPa
Concrete compressive strength	f_{cm}	28	MPa
Concrete Young's modulus	E_c	30	GPa
Reinforcement Young's modulus	E_s	200	GPa
Cross sectional area of the entire bar	A_c	0.1·0.1	m^2
Cross sectional area of the reinforcement bar, 1φ16	A_s	$2 \cdot 10^{-4}$	m^2

The effective cross sectional area of the uncracked parts of the bar, $A_{I,eff}$, are calculated as follows:

$$A_{I,eff} = A_c + (E_s/E_c - 1)A_s = 0.01 + (200 \cdot 10^9/30 \cdot 10^9 - 1) \cdot 2 \cdot 10^{-4}$$

$$A_{I,eff} = 0.0111\ m^2$$

1. Determine whether the bar cracks or not

Calculate stress with the assumption of no cracks and compare with the concrete strength.

$$\sigma_c = \Delta T \alpha E_c = 10 \cdot 10^{-5} \cdot 30 \cdot 10^9 = 3\ MPa\ >\ f_{ct}$$

I.e. the bar will crack

2. Determine whether there will be more than one crack

Assume that one crack has formed and use deformation compatibility in order to determine the concrete stress in uncracked sections.

Perceived elongation of the bar at $\Delta T = -10°C$:

$$\Delta L = \Delta T \alpha L = 10 \cdot 10^{-5} \cdot 2 = 2 \cdot 10^{-4} m$$

This elongation shall correspond to the sum of the elongation of the uncracked length of the bar and the crack width. The crack width is expressed using Eq. (4.2).

$$\Delta L = 2 \cdot 10^{-4} = \varepsilon_R L + w(F)$$

$$\Delta L = \frac{FL}{E_c A_{I,eff}} + \left(0.420 \left(\frac{\varphi F_S^2/A_S^2}{0.22 f_{cm} E_S \left(1 + \frac{E_S\ A_S}{E_c A_{I,eff}}\right)} \right)^{0.826} + \frac{F_S}{A_S E_S} 4\varphi \right) /1000$$

The force is constant along the bar, i.e. $F = F_s$.

$$2 \cdot 10^{-4} = \frac{2F}{30 \cdot 10^9 \cdot 0.0111} + \left(0.420 \left(\frac{16 \cdot F^2/\left(2 \cdot 10^{-4}\right)^2}{0.22 \cdot 28 \cdot 10^6 \cdot 200 \cdot 10^9 \cdot \left(1 + \frac{200 \cdot 10^9}{30 \cdot 10^9} \cdot \frac{2 \cdot 10^{-4}}{0.0111}\right)} \right)^{0.826} + \right.$$

$$\left. + \frac{F}{2 \cdot 10^{-4} \cdot 200 \cdot 10^9} 4 \cdot 16 \right) /1000$$

$$\rightarrow F = 18.2\ kN$$

The corresponding stress in the concrete at uncracked sections thus becomes

$$\sigma_c = F/A_{I,eff} = 18.2 \cdot 10^3/0.0111 = 1.64\ MPa\ < f_{ct}$$

I.e. only one crack will form.

3. Calculate the crack width for the obtained force in the bar

The crack width is calculated using Eq. (4.2) with the restraint force inserted.

$$w_m = 0.420\left(\frac{16\cdot 18200^2/\left(2\cdot 10^{-4}\right)^2}{0.22\cdot 28\cdot 10^6\cdot 200\cdot 10^9\cdot\left(1+\frac{200\cdot 10^9}{30\cdot 10^9}\cdot\frac{2\cdot 10^{-4}}{0.0111}\right)}\right)^{0.826} + \frac{18200}{2\cdot 10^{-4}\cdot 200\cdot 10^9}\cdot 4\cdot 16$$

$$w_m = 0.091\ mm$$

Calculation without any consideration of stress reduction due to cracking:

If the stress reduction due to cracking is disregarded, the crack width is calculated directly from the stress obtained when not including any cracking, i.e. assuming σ_c = 3 MPa. The reinforcement stress in the crack is then calculated using force compatibility along the bar:

$$\frac{\sigma_c A_{I,eff}}{A_S} = \sigma_s \leftrightarrow \frac{3\cdot 10^6\cdot 0.0111}{2\cdot 10^{-4}} = 167\ MPa$$

The crack width w_m can then be calculated using Eq. (4.2):

$$w_m = 0.420\left(\frac{\varphi\sigma_s^2}{0.22 f_{cm} E_s\left(1+\frac{E_S\ A_S}{E_c A_{eff}}\right)}\right)^{0.826} + \frac{\sigma_s}{E_s}4\varphi$$

$$w_m = 0.420\left(\frac{16\cdot\left(167\cdot 10^6\right)^2}{0.22\cdot 28\cdot 10^6\cdot 200\cdot 10^9\left(1+\frac{200\cdot 10^9\cdot 2\cdot 10^{-4}}{30\cdot 10^9\ \cdot 0.0111}\right)}\right)^{0.826} + \frac{167\cdot 10^6}{200\cdot 10^9}4\cdot 16$$

$$w_m = 0.22\ mm$$

I.e. more than twice as large as the crack width when considering restraint effects.

Example 1 illustrates the difference in crack widths when calculated with the two different methods, including or disregarding the reduction of restraint due to cracking. In order to further demonstrate the difference between the methodologies, the restraint force and crack widths of the entire process of cracking is also calculated. The results are shown in Fig. 4.6, and the lines denoted "Standard method" and "Uncracked stiffness" are based on the same methodologies as in Example 1. However, the calculations are also made using a third method, denoted "Spring method". In this method, the bar is divided into springs similar to what was shown in Fig. 4.3. The springs representing uncracked concrete have the initial stiffness attributes, and the

springs representing the cracks have the stiffness of the reinforcement only. The length of the springs representing the cracks is based on the transfer length calculated using Eq. (4.3).

As the influence of the concrete gradually increases along the transfer length when moving away from a crack, the springs representing the crack cannot correspond to the full transfer length on both sides of the cracks, i.e. $2 \cdot l_t$. A more reasonable assumption would be to assume that half the transfer length on each side of the crack has the stiffness of reinforcement only, and the other half has the stiffness of the uncracked cross section. In the development of the method, a calibration of the length of the springs with crack properties was made, using test results of reinforced concrete bars subjected to increased elongation, presented in Jansson (2011) and Jansson et al. (2012). In the calibration, the length of the springs representing the cracks was adjusted to $1.05 \cdot l_t$.

As the "Spring method" calculates the transfer length, the method can easily be used to check if the stabilized crack pattern is reached. In the "Standard method", the number of cracks is not limited in the same way, as the transfer length is not used. For this reason, the "Standard method" calculations were aborted when there should be no more room for a new crack.

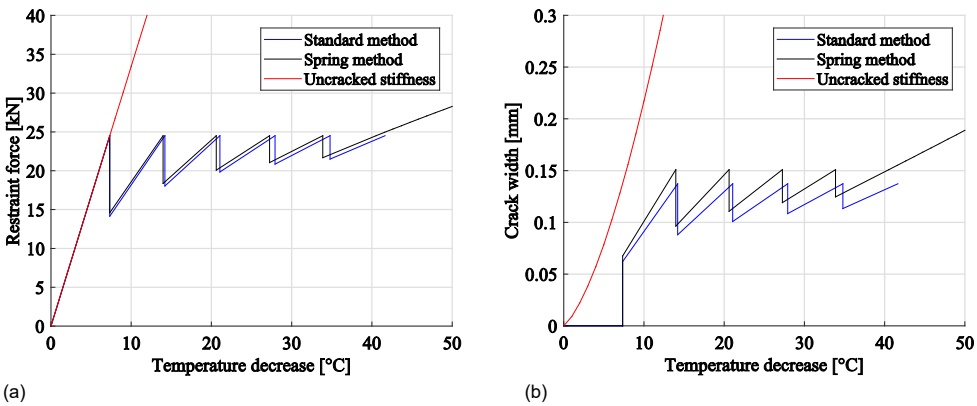

Fig 4.6. Diagram showing the restraint force (a) and crack width (b) in the bar in Example 1 as a function of the temperature decrease.

A simplified way to consider cracking in end restrained structures is suggested in Eurocode 2-3 (CEN, 2006), which regards design of liquid retaining structures. The document presents a design method in which the crack width is calculated for the stress which causes cracks to form, i.e. the expression gives the maximum crack width possible during the crack formation stage. This can be a reasonable simplification as long as it can be assumed that the stable crack pattern is not reached.

4.3.2 Base restrained walls and portal frame bridges

In the previous section where end restrained reinforced concrete bars were considered, the restraint effect was constant in the entire specimen. However, in the case of edge restrained specimens, the degree of restraint varies within the specimen, as was shown in Fig. 3.2. This means that the location of the first crack is not random, but is more likely to appear in an area with a high degree of restraint. When a crack has formed, the concrete beside it contracts, which reduces the restraint stresses in the area beside the crack. However, the restraining edge as well as the reinforcement limits the contraction of the concrete. In this way, the edge restraint not only causes cracks to form, but also limits their width. For this reason, the maximum crack width in base restrained walls is often not found at the base, where the degree of restraint is largest, but further up in the walls. This was seen in tests of cracking in reinforced base restrained walls performed by Stoffers (1978), Kheder et al. (1994), Kheder (1997) and Micallef et al. (2017).

The varying degree of restraint and the non-uniform reduction of restraint stresses due to cracking makes it difficult to analyze cracking in base restrained walls analytically. Analytical expressions for crack widths are however listed in e.g. Kheder et al. (1994). Eurocode 2-3 (CEN, 2006) suggests an expression in which the difference in strain along the transmission length given in Eurocode 2-1-1 (CEN 2005a) and shown in Eq. (2.3), is replaced by the expression shown in Eq. (4.7). In the equation, R is the degree of restraint and ε_{free} is the strain which should occur if the element was unrestrained. The document also prescribes values of the degree of restraint, which equals 0.5 in the bottom parts of the walls. However, Bamforth et al. (2010) argues that the crack width does not have as strong dependency of the restrained strain ($R\varepsilon_{free}$) as suggested by CEN (2006), and suggests another expression for calculation of crack widths in base restrained walls. It should also be noted that no analytical expression for crack widths due to restraint effects in base restrained walls is included in Eurocode 2-1-1, which regards design of concrete structures in general, or Eurocode 2-2, which regards design of bridges.

$$(\varepsilon_{sm} - \varepsilon_{cm}) = R\varepsilon_{free} \tag{4.7}$$

FE-analyses have also been used to investigate cracking in base restrained walls. FE-models have previously been developed and presented in e.g. Kianoush et al. (2008) and Matinmanesh and Kianoush (2013) for this purpose, who used the test results of Kheder (1997) to verify their model, and in Micallef et al. (2017), who verified the model using the test results presented in the same paper. A portal frame bridge as illustrated in Fig. 2.2 can be considered as a group of structural elements connected to each other along one or two edges, as discussed in section 3.1. A model which can predict cracking due to restraint in base restrained walls could therefore also be used to illustrate cracking in portal frame bridges, after some modifications.

4.3.3 Influence of creep

Creep describes the increase in deformations that occur over time when structures are subjected to long-term loading. If a structure is subjected to restraint effects, creep will instead lead to a gradual decrease of stresses in the structure. In design calculations, creep effects are often considered as a reduction of Young's modulus, as shown in Eq. (4.8), where E_c is the initial Young's modulus, ϕ is the creep coefficient and $E_{c,eff}$ is Young's modulus with consideration taken to creep effects. The development of creep over time is thereby disregarded in the calculations, and the final deformation (or the stress value, in restraint situations) is instead determined directly from the load effect (or the imposed strain, in the case of restraint) (Ljungkrantz et al., 1994).

$$E_{c,eff} = \frac{E_c}{1+\phi} \tag{4.8}$$

As cracking occurs for a certain stress value in the concrete, the assumption of creep thus means that a larger restrained strain is required in order to cause cracking. In reinforced concrete, this larger strain will cause a larger stress in the reinforcement before cracking occurs, which means that the cross-sectional force required to cause cracking increases. This in turn leads to an increase of crack widths. This is illustrated in Fig. 4.7, which shows the restraint force and crack widths in the same reinforced concrete bar as in Example 1 and Fig. 4.6, using the "Spring method" for calculation, but with different creep coefficients. Results from a similar comparison is shown by Nesset and Skoglund (2007).

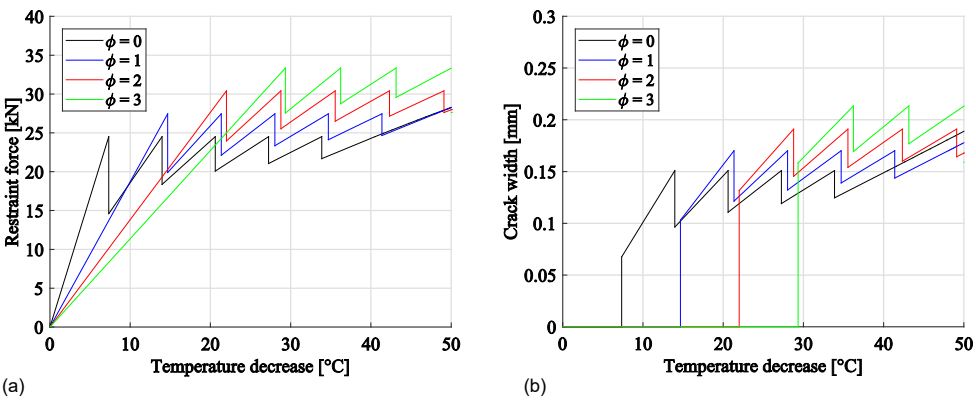

Fig 4.7. Diagram showing the restraint force (a) and the crack width (b) in the bar in Example 1 as a function of the temperature decrease, for four different values of creep.

In linear elastic design models, the reinforcement is generally omitted, as the required amount of reinforcement is to be decided. Omitting the reinforcement means that the increase in force and thus crack widths is not captured when creep is considered as a reduction of Young's modulus according to Eq. (4.8). Such an analysis can thus capture

the restraint effect required for cracking correctly (assuming the creep coefficient is correct and cracking does not occur before the creep has developed), but will underestimate the resulting crack widths. Also, subsequent cracking is delayed, as the reduction of the restraint force due to cracking is overestimated. This is illustrated in Fig. 4.8, which shows the restraint force and crack widths for the cases with $\phi=0$, $\phi=1$ and estimating $\phi=1$ by halving the load effect in the model. The reduction of the load effect is in this case achieved by halving the coefficient of thermal expansion. This reduction of the load effect corresponds to halving the Young's modulus (i.e. assigning $\phi=1$) in a linear elastic model which do not include reinforcement.

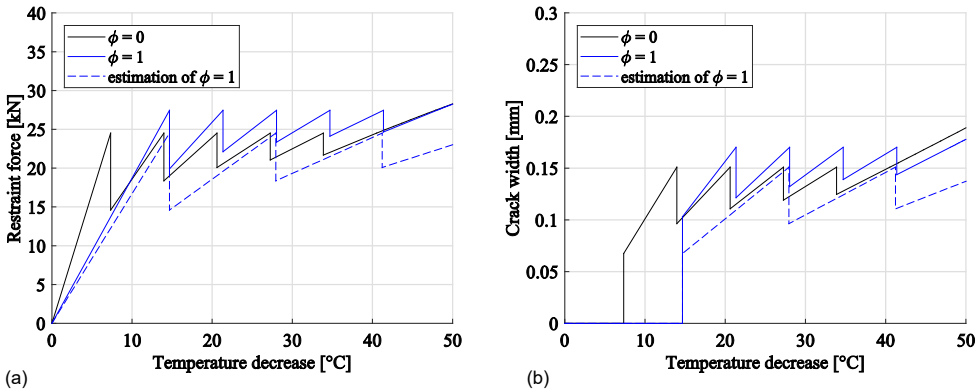

Fig. 4.8. Diagram showing the restraint force (a) and the crack width (b) in the bar in Example 1 for different values of creep and different methods of considering creep in the model.

4.4 Investigation of cracking using FE-analyses

In this study, cracking in base restrained walls and portal frame bridges were investigated using FE-analyses. When analyzing base restrained walls, the concrete was modeled with plane stress elements, and the bi-linear material behavior suggested by Gylltoft (1983) was used for concrete in tension. The reinforcement bars were modeled as discrete bars, and the bond-slip relation presented in Eq. (4.1) was used to describe the stress transfer between the materials.

A fixed crack direction with a shear retention of 0.3 was used, which rendered realistic results in initial analyses and also lead to few convergence difficulties. The interface between the surfaces of the concrete structural parts as well as between the bottom surface and the ground were modeled using non-linear interface elements. A more detailed description of the model used for analyses of base restrained walls is given in paper V.

In paper V, the analysis model was validated by re-creating results of full-scale tests of base restrained walls presented in Micallef et al. (2017) and Kheder (1997), which showed that the analysis model tends to overestimate both the number of cracks and the crack widths. This is considered acceptable, as an overestimation of cracking will lead to conservative conclusions regarding the reinforcement amounts required for limitation of crack widths. There are several modeling aspects which can explain the difference between test and analysis results. Some examples are that the analysis did not include the material development during the curing phase, there were uncertainties regarding the material parameters and the stiffness of the connections, and that the analysis model was a 2D-model. The fact that the walls were modeled in 2D indicates that only through cracks can appear in the model, and that the entire cross-sectional area constitutes the effective cross sectional area. The difference between analysis results and test results can also be due to uncertainties in the tests, e.g. the stiffness of the connection towards the foundation. In the comparison with the tests in Kheder (1997), several material parameters required in the FE-analyses were unknown.

Another comparison of results was made with the analysis results of crack widths in base restrained walls by Zangeneh Kamali et al. (2013), who presented crack widths in five fictitious walls subjected to thermal actions. The height of the walls was 3 m and the width varied from 3 m to 21 m. The cross-sectional thickness was 0.5 m, and the walls were reinforced with φ12 cc 125 mm in both vertical and horizontal direction, and on both sides of the system line. The walls were restrained from horizontal movements along the top edges. Zangeneh Kamali et al. (2013) compared the resulting crack widths with crack widths calculated for the walls with the methodology presented in Eurocode 2-3 CEN (2006). The comparison showed the crack widths in Zangeneh Kamali et al. (2013) and Eurocode 2-3 CEN (2006) to be of similar magnitude.

The analyses performed in Zangeneh Kamali et al. (2013) were re-created in this study using the model developed in paper V, which rendered fewer and wider cracks compared to the original analyses. The models were slightly different as Zangeneh Kamali et al. (2013) assumed a rigid connection between reinforcement and concrete and used quadratic elements, whereas the model developed in paper V uses a bond-slip relation for concrete – reinforcement interaction and uses triangular elements. The bi-linear relations used for the descending part of the concrete stress-strain relations in tension were also slightly different. The difference in results is illustrated by comparing Figs. 4.9 and 4.10, as Fig. 4.9 shows the crack pattern and crack widths presented in Zangeneh Kamali et al. (2013), and Fig. 4.10 shows the results obtained in this study. Note that the color scale is different in the two figures. The comparison illustrates the relatively large differences in results that can be obtained when non-linear FE-analyses with slightly different modeling choices are used to model cracking in reinforced concrete.

Fig. 4.11 shows the corresponding results from when the bond-slip relation in the analysis in this study was replaced with a rigid connection between concrete and reinforcement. This type of reinforcement to concrete interaction was used in Zangeneh Kamali et al. (2013), and it can be seen that these analyses agree better with the results in Fig. 4.9, especially in terms of crack widths. The number of cracks was also increased when the bond-slip relation was replaced with a rigid connection, which can explain the reduced crack widths. Using a bond-slip relation thereby leads to fewer and wider cracks in the investigated cases, which is considered unfavorable. This significant effect of introducing bond-slip was also seen in paper V.

The direction of the cracks is also different from the analyses by Zangeneh Kamali et al. (2013), which was shown to be caused by the element shape. The quadratic elements used by Zangeneh Kamali et al. (2013) rendered vertical cracks, while the triangular elements used in this study rendered more inclined cracks. Quadratic elements were also tested in this study, which then rendered vertical cracks also in this case. As the cracks were inclined in the analyses made in this study, the crack widths shown in Fig. 4.10 and 4.11 are perpendicular to the crack direction, and not in the horizontal direction as in Fig. 4.9.

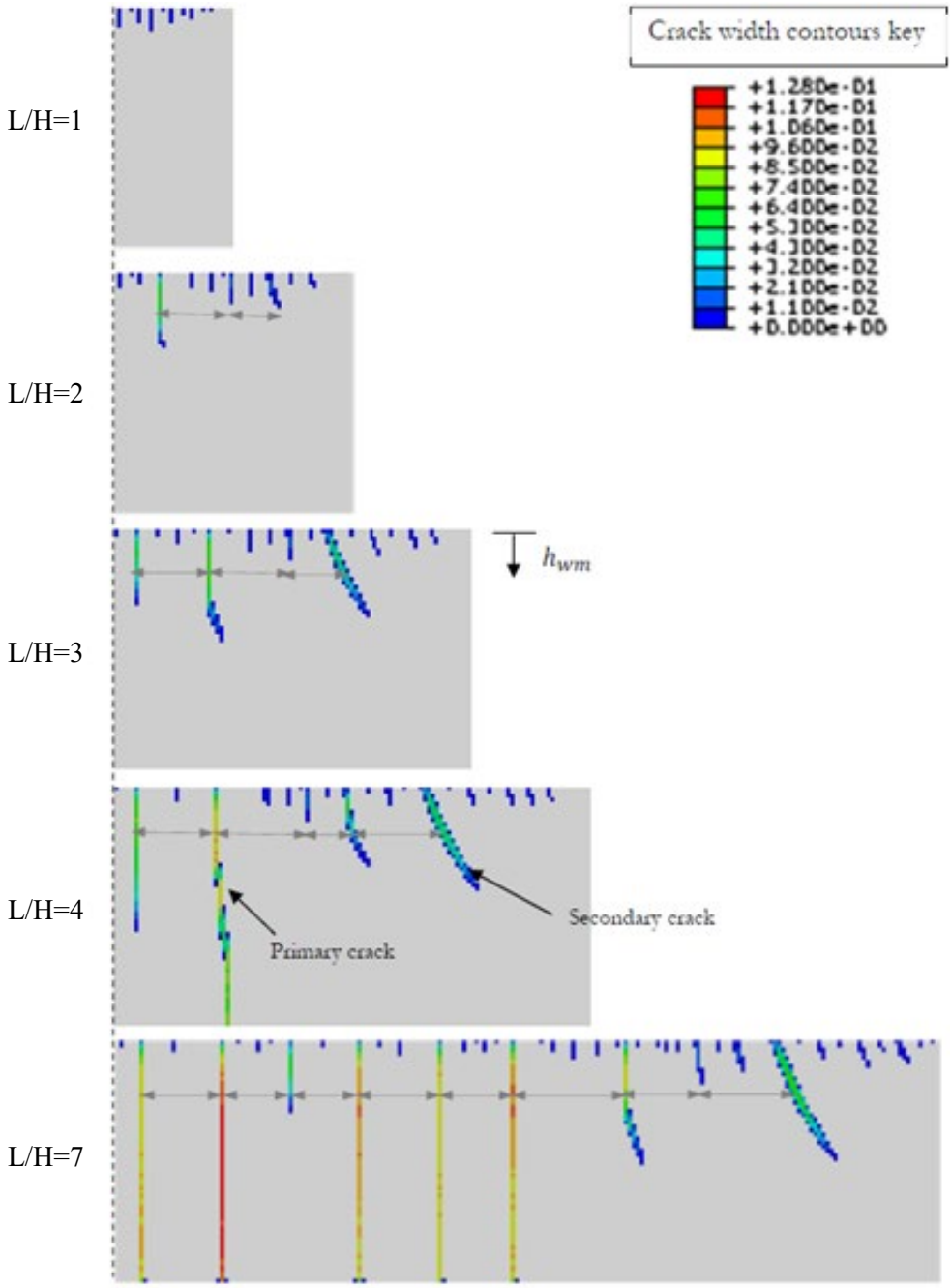

Fig. 4.9. Results from analyses of cracking in base restrained walls presented in Zangeneh Kamali et al. (2013). The maximum crack width is 0.128 mm.

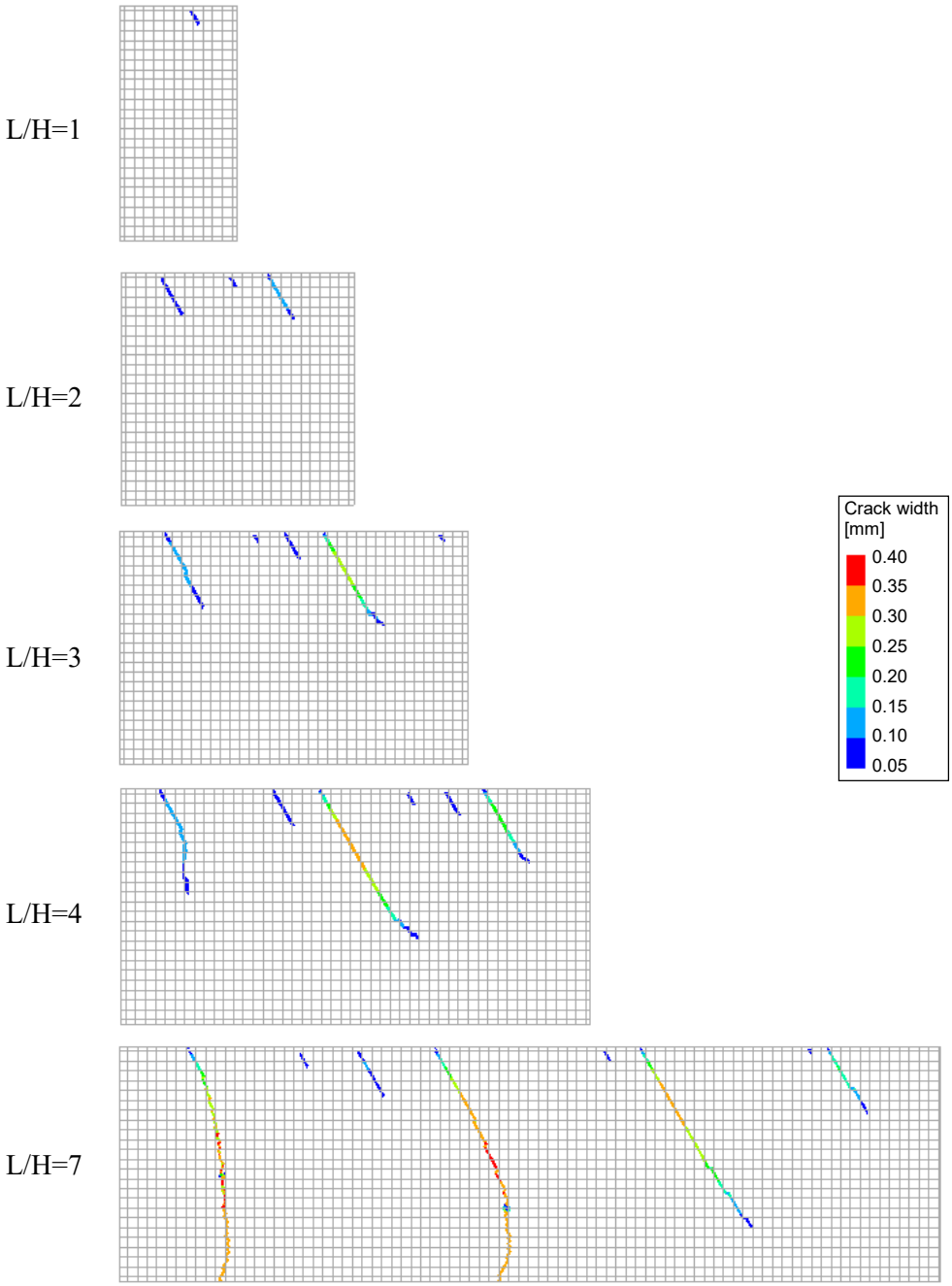

Fig. 4.10. Results from analyzing the same fictitious walls as in Fig. 4.9 using the model developed in paper V. The grids seen in the walls illustrate the reinforcment bars. The maximum crack width is 0.40 mm.

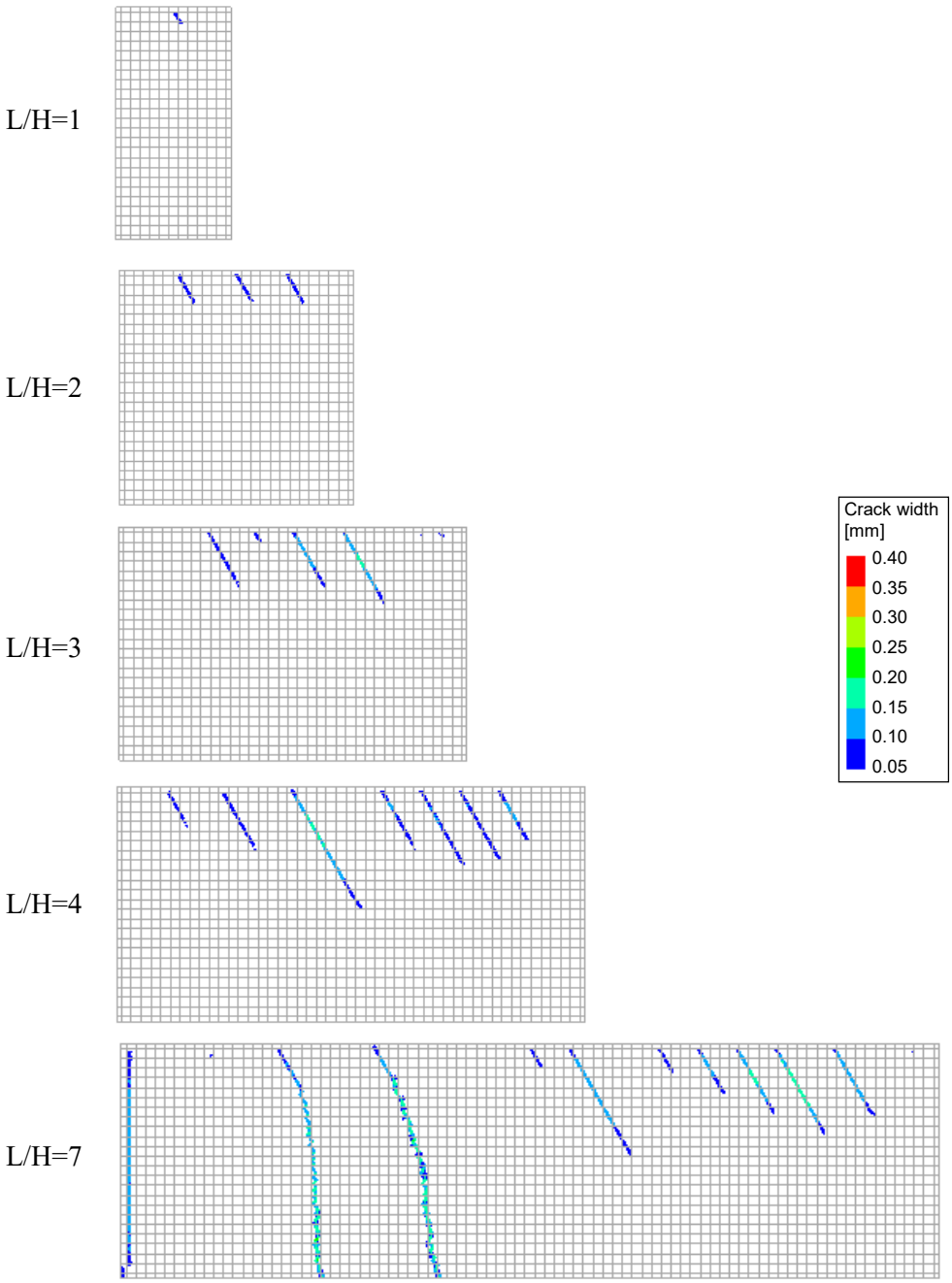

Fig. 4.11. Results from analyzing the same fictitious walls as in Fig. 4.9 using the model developed in paper V, but using embedded reinforcement instead of bond-slip relations. The grids seen in the walls illustrate the reinforcment bars. The maximum crack width is 0.19 mm.

The results of Zangeneh Kamali et al. (2013) indicated that the calculations in CEN (2006) renders reasonable results, as the maximum crack width in the analysis was 0.13 mm and the crack widths calculated using CEN (2006) was 0.15 mm. It should be noted that the analytical crack width was in this case calculated assuming $R=1$, which was also used in the analysis, while $R=0.5$ is recommended in CEN (2006). Also, the expression recommended in Eurocode for the crack distance ($s_{r,max}$) was used instead of the Swedish national choice, presented in Eq. (2.2).

The crack widths in Zangeneh Kamali et al. (2013) are however significantly smaller than the crack widths found in the present study, as can be seen by comparing Figs. 4.9 and 4.10, and considering the changed color scale. Fig. 4.12 shows the maximum crack widths during the analyses presented in Fig. 4.10, as well as the result calculated using CEN (2006), i.e. Eqs. (2.1), (2.3) and (4.7), with $R=1$. It can be seen that the results obtained in this study are not consistently smaller than the results obtained using the analytical expression. Also, the crack widths are not proportional to the thermal action, but may decrease when an additional crack appears in the wall, as was also stated by Bamforth et al. (2010). This would have been even more visible in Fig 4.12 if results were shown with smaller intervals of thermal action than 1°C.

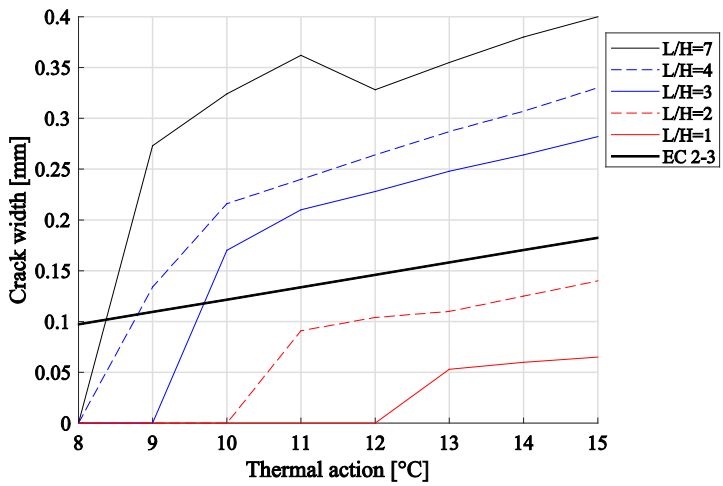

Fig. 4.12. Development of crack widths in analyses in this study using bond slip, and comparison with theoretical result calculated with Eqs. (2.1), (2.3) and (4.7), with $R=1$.

The findings of a few wide cracks instead of several smaller cracks using the model developed in this study is also in accordance with observed cracking in some portal frame bridges in Sweden, which is reported in BaTMan (Trafikverket, 2018). One example is bridge 1280-264-1 in Malmö, which was built in 1962. In an inspection in august 2009, a single 1.0 mm wide vertical crack was observed in both abutments, which has also been seen and measured to the same width in inspections in April 2013, October 2015 and September 2018. Another example is bridge 1280-367-1, also in

Malmö, built in 1998. A single 0.4 mm wide vertical crack was noted in its abutments in September 2009. The cracks were later injected but opened again and were measured to 0.4 mm in inspections in 2013 and September 2015. However, the cause of cracking in these cases and the reinforcement layout used in the bridges have not been investigated within this study.

4.5 FE-analyses of cracking in portal frame bridges

After the model for cracking in base restrained walls was validated, it was used to investigate cracking in portal frame bridges. In these analyses, curved shell elements were used in place of plane stress elements, as stresses were no longer limited to a plane. Interface elements with a bed stiffness of 50MN/m^3 were placed under the foundation, which represented the vertical stiffness of the soil. The soil was however not limiting expansions in the longitudinal or transversal direction, see Fig. 2.2.

The actions included in the analyses were self-weight of the concrete and the soil upon the foundations, shrinkage differences due to casting of the structure in stages, described in section 3.3, and the thermal load case presented in Fig. 3.8. Horizontal stresses induced by the soil were omitted from the analyses, although e.g. horizontal soil pressure on the wing walls could cause transverse stresses in the abutments. These stresses would however become larger due to uniform shrinkage combined with a uniform thermal action, which are not investigated within this research project.

The self-weight was applied first, and was needed in order to cause realistic deformations of the foundation. Thereafter, the difference in shrinkage was applied, as it is a permanent action. Then, the characteristic value of the thermal action was applied, in order for cracking to occur. Finally, the thermal action was reduced to its quasi-permanent value, as crack widths shall be determined using a quasi-permanent load combination.

The risk for cracking and the resulting crack widths were investigated both in the frame corner and in the bottom of the abutment, close to the foundation. Cracking in the foundation itself was however not investigated, as the geometry of the foundation can vary significantly, which makes it difficult to draw any general conclusions regarding the cracking. Creep effects were not included in the analyses in this section. A detailed consideration of creep is difficult as it develops over time. A simplified way of including creep in the analyses is to reduce the load values, which gives similar effects as reducing the Young's modulus of the concrete. However, as was shown in section 4.3.3, including creep this way can render an accurate time for the formation of the first crack, but the resulting crack widths will be underestimated. Also, subsequent cracking is delayed. Therefore, this method of inclusion of creep was considered unreliable. Creep was however included as a reduction of loads in paper VI.

The structural model used is shown in Fig. 4.13. The bridge was given a relatively large width, which leads to larger degrees of restraint in the structure. The width was however reduced in some analyses. The cross-sectional height was 0.4 m in the bridge deck and in the abutments, and 0.5 m in the foundations. The concrete was of quality C40. Double symmetry was utilized, i.e. only a fourth of the bridge is modelled.

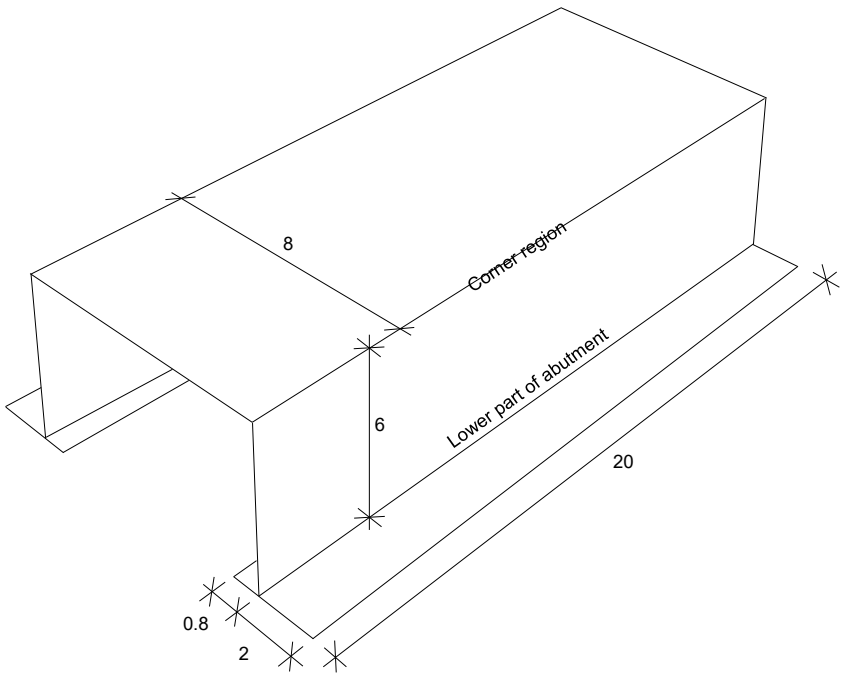

Fig. 4.13. Structural model of bridge used in analyses of cracking. Dimensions in m.

4.5.1 Cracking in the corner region

The restraint effects investigated in this study were less prone to cause cracking in the corner region than in the lower part of the abutment, as the thermal actions were smaller in the corner region, and no difference in shrinkage was occurring. Initially, analyses using linear elastic material models were made, in which the characteristic thermal load was also applied. These analyses were meant to indicate in which cases cracking may occur in the corner region at all. The analyses showed that the load case in Fig. 3.8 caused larger tensile stresses in the top part of the abutment when the bridge deck is warm, than in the bridge deck when the bridge deck is cold. The reason for this is that the temperature difference between abutment and foundation caused compressive stresses in the entire corner region when the foundation was warm, but caused tensile stresses in the corner region when the foundation was cold.

Correspondingly, it was found that including the difference in shrinkage caused compressive stresses in the entire corner region.

In order not to underestimate the risk of cracking, analyses of the risk for cracking in the bridge deck were therefore run with the temperature difference between bridge deck and abutment only, while the entire thermal load case was included when investigating cracking in the top of the abutment, and shrinkage was omitted in both cases. In order to determine whether cracking might occur, the stresses resulting from the analyses were compared with the characteristic tensile strength of the concrete, which was 2.5 MPa.

The largest tensile stress occurring in the bridge deck for the characteristic load values was found to be 1.75 MPa, which is well below the tensile strength of 2.5 MPa. When the temperature difference between abutment and foundation also was applied, the maximum tensile stress in the bridge deck was reduced to 1.05 MPa. Adding the difference in shrinkage between foundation and bridge deck to the two temperature differences reduced the maximum tensile stress to 1.00 MPa. For this reason, cracking in the bridge deck due to the investigated load effects was considered as unlikely. The concrete strength could however be reduced by self-equilibrating stresses resulting from the curing, which combined with the investigated load effect could case cracking. This effect was however omitted in this study, as it is generally omitted in design situations. Also, as mentioned in section 3.2.5, the cross-sectional height of bridge decks is sometimes larger than the abutments, while the opposite is very unusual. Having a larger cross-sectional height in the bridge deck than in the abutment would reduce the degree of restraint in the bridge deck, which in turn would reduce the tensile stresses even further.

On the other hand, the maximum tensile stress in the top of the abutment in the analyses was 3.0 MPa. As this value is larger than the characteristic tensile strength of the concrete, it was assumed that cracking could occur. Therefore, non-linear FE-analyses were made in order to investigate the resulting crack widths. In the non-linear analyses, the mean values of the concrete material properties were used, as the analyses were to capture the actual behavior of the material. However, as the mean tensile strength of the concrete is higher than the maximum tensile strength in the linear elastic analyses, the thermal actions were increased by a factor of 1.4. The factor value corresponds to the difference between mean and characteristic strength of concrete C40, and assures that cracking will occur in the analyses.

Analyses were made using the model of a 20 m wide bridge shown in Fig. 4.13, as well as with a model in which the width was reduced to 10 m. Minimum reinforcement according to Eq. (2.4) was placed in the abutment, corresponding to φ16 cc 195 mm both horizontally and vertically and on both sides of the cross sectional system line. In Eq. (2.4), k was calculated using the Swedish national choice presented by Boverket (2015), rendering the value $k=0.733$. The results of the analyses are shown in Fig. 4.14.

In the analysis of the 10 m wide bridge, only one crack appeared, which formed beside the symmetry line and reached a maximum width of 0.10 mm. The fracture energy of this row of elements was halved in order to account for the equal crack forming on the other side of the symmetry line. By halving the fracture energy, it was considered that the entire crack width was captured in the model. When the bridge was 20 m wide, two cracks formed, one beside the symmetry line and the other about 3.7 m away from it. The maximum crack width was in this case 0.12 mm.

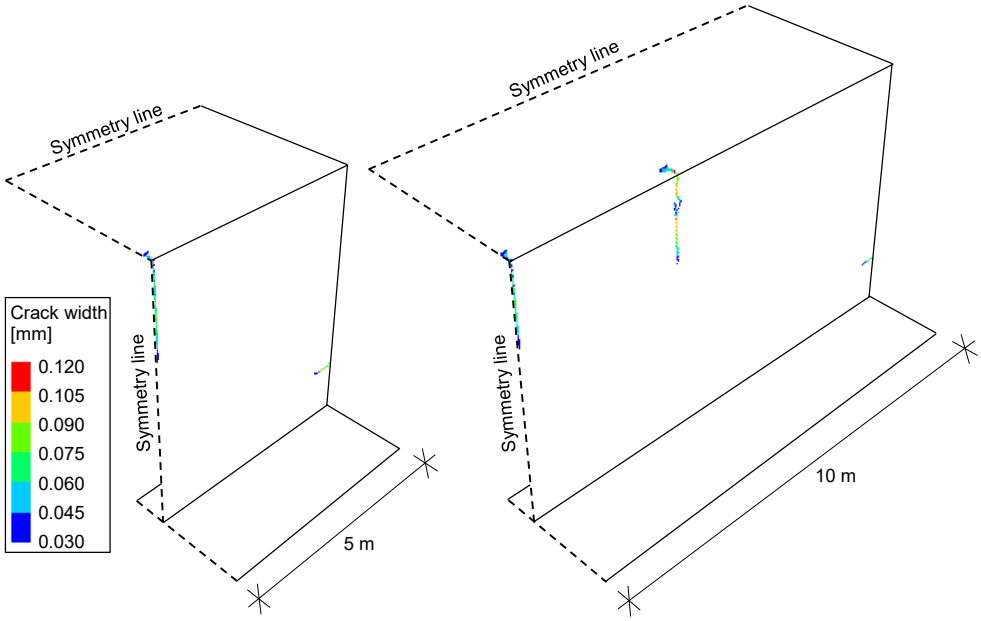

Fig. 4.14. Crack patterns and crack widths when cracking in the top edge of the abutment was investigated. Results are shown for the quasi-permanent load combination, after the thermal load has been reduced from its characteristic value.

The characteristic crack width, which shall be compared with the demands on crack width limitation, is calculated as the mean crack width multiplied with 1.3, as shown in Eq. (4.4). In this case, the largest crack width in each wall multiplied with 1.3 renders crack widths of 0.13 mm and 0.16 mm, respectively. Choosing the maximum crack width from the analyses for use as w_m in Eq. (4.4) is meant to add a safety margin to the result. As crack width limitations are often 0.15 mm or 0.20 mm (see section 2.1.1), it can be concluded that the load case combined with minimum reinforcement according to Eq. (2.4) can lead to crack widths close to the limit of what is considered as being acceptable. A small investigation of the influence of the reinforcement amount on the crack widths was made, by halving the transverse reinforcement in the model. The reinforcement amount was found to have a relatively small impact on the result, as the characteristic values of the maximum crack widths increased to 0.14 mm and 0.18 mm, respectively, and cracks formed in roughly the

same locations. This indicates that the reinforcement amount does not have as large influence on the crack widths as in non-restraint cases.

When evaluating the results presented in this section, the following should be kept in mind:

- The relative cross-sectional heights of the structural parts affect the degree of restraint. If the parts have different cross-sectional height, the part with smaller cross-sectional height is more prone to cracking. As abutments are in some cases made with smaller cross-sectional heights than bridge decks, especially in bridges with long spans, this likely increases the crack widths in the abutments.
- For the investigated cases, the stress variations over the cross-sectional height were small, and the cracks forming in the analysis model were through cracks.
- The use of shell elements means that stress transfer in the direction of the cross-sectional height is not modeled. This means that in the model, the entire cross-sectional height is considered as the effective cross-sectional height. For the specific structural model investigated in this study, this had only a small impact on the result, as the cross-sectional height was 400 mm and the cover 72 mm on both sides. However, using the model in cases where there is a significant difference between the effective concrete area and the total area would mean that secondary cracks, which are forming within the effective concrete area and are caused by the restraining effect of the reinforcement (Schlicke and Tue, 2015), is omitted. This will likely lead to an underestimation of the total number of cracks, and thus to an overestimation of crack widths.
- Residual stresses from the curing phase were omitted in the study. This could lead to an underestimation of crack widths, as shown in paper V. However, disregarding residual stresses from the curing phase is common in design situations.
- There is a large degree of randomness regarding cracking, which implies that there is a risk of underestimating the maximum crack width in specific cases. For this reason, the characteristic crack width is compared with the limit values, instead of the mean crack width. However, as the model has not been validated for portal frame bridges, it is unclear whether this safety margin is sufficient. Possibly, an additional safety margin could be assigned to the calculation results.

In conclusion, it is likely that the bridge decks of portal frame bridges will not crack due to differences in temperature between the structural parts. The top part of the abutments may however do so, and the cracks might become wider than allowed, especially if the abutment cross-sectional height is smaller than that of the bridge deck.

If instead a linear elastic analysis is made, the stresses resulting from the quasi-permanent load case determines the required reinforcement amount. With the bridge geometry presented in Fig. 4.13, the tensile stresses in the concrete in the middle of the cross section were smoothed out according to Trafikverket (2011b) and multiplied with the cross-sectional height, in order to obtain the force that should be carried by the reinforcement. The reinforcement amount required for crack width limitation was thereafter calculated using the conventional design method (Eqs. (2.1–2.3)). The maximum smoothed out tensile stresses in the concrete were 0.47 MPa in the bridge deck and 0.79 MPa in the abutment, and the reinforcement required to limit crack widths to 0.15 mm in the two cases was φ16 cc 130 mm and φ16 cc 98 mm, respectively, on both sides of the system line. A 15°C temperature difference between structural parts was also assigned to the structure, as in the conservative interpretation of the Eurocode load case (see Fig. 3.7 (c) and (d)). The resulting maximum smoothed out stresses were in this case 2.1 MPa in the bridge deck and 3.7 MPa in the abutment, rendering a reinforcement need of φ16 cc 57 mm and φ16 cc 40 mm, respectively, on both sides of the system line.

A comparison was also made between the reinforcement amounts used in the non-linear analyses and the amount of reinforcement required to obtain the same crack width when using the new thermal load case in the linear elastic analysis, combined with the conventional crack width calculation method (Eqs. (2.1–2.3)). The results were compared by calculating a factor describing the difference in reinforcement amounts, by dividing the cc-distance in the non-linear analysis with the cc-distance resulting from using the conventional design method. The results are shown in Table 4.3, which summarizes the characteristic crack widths from the four different analyses. The stress values from the linear elastic analyses are independent of the reinforcement amount, as the reinforcement is not included in the linear elastic analysis. The difference in required cc-distance between the cases where the same bridge width is therefore only due to the difference in the crack width that should be obtained.

The results show that the factor describing the difference in reinforcement amounts can vary significantly when the reinforcement amount is changed. It can also be noted that the factor gets slightly smaller when the width of the bridge is increased. However, too few analyses were made for general conclusions to be drawn.

Table 4.3. Comparison of crack widths in non-linear analyses, reinforcement required to obtain the same crack widths using the conventional design method and the factor describing the difference in reinforcement amounts.

Analysis model	10 m wide cc 195 mm	20 m wide cc 195 mm	10 m wide cc 390 mm	20 m wide cc 390 mm
Char. crack width in non-linear analysis [mm]	0.13	0.16	0.14	0.18
Tensile stress used in conventional crack width calculation [MPa]	0.69	0.79	0.69	0.79
Required cc to obtain same crack width with conventional method [mm]	98	102	102	109
Factor describing difference in reinforcement amount	2.0	1.9	3.8	3.6

4.5.2 Cracking in the lower part of the abutment

In the lower part of the abutment, linear elastic analyses, including both the characteristic values of the thermal load case and the difference in shrinkage, caused stresses of up to 7 MPa. It is therefore obvious that the characteristic load values will cause cracking in this area, and extensive non-linear analyses were therefore made in order to investigate the cracking further. These analyses were performed without utilizing the symmetry condition in the width direction of the bridge, as it had been shown that utilizing symmetry could affect the number of cracks in the abutment. As the first crack appeared beside the symmetry line due to the reduced fracture energy, the number of cracks in the entire wall would always become uneven in such a model. The structural model used was the same as in the previous section, with the exception of the width of the wall, which was reduced to 10 m. This was done in order to limit the size of the model.

Seven analyses were made using different cc-distances for the reinforcement in both vertical and horizontal direction. φ16 and identical reinforcement on both sides of the system line was used also in this case. The resulting maximum characteristic crack widths are shown in Fig. 4.15, as a function of the cc-distance. In a corresponding linear elastic analysis using quasi-permanent loads, the largest transverse tensile stress value was 2.7 MPa after being smoothed out according to Trafikverket (2011b). The crack width calculated from this result using Eqs. (2.1–2.3) is also shown in the figure as a function of the cc-distance. As can be seen in the figure, the factor describing the difference in reinforcement required to obtain the same crack widths in the conventional design method and the non-linear analyses increases with reduced reinforcement ratio in the non-linear analysis. The factors describing the difference in reinforcement amounts, as well as the characteristic crack widths for quasi-permanent load in the non-linear analyses and the cc-distances required to obtain the same crack widths in the conventional method are shown in Table 4.4.

It can be seen in Table 4.4 that when the minimum reinforcement is used, which corresponds to φ16 cc 195 mm on both sides of the cross section, the characteristic crack width (0.34 mm) is larger than the limit values for crack widths in Swedish bridges (0.15–0.20 mm, see section 2.1). It should however be noted that the crack width resulting from the analysis is dependent on the bridge geometry, i.e. no general conclusion could be drawn from the results. Also, along edges where differences in shrinkage due to casting of the bridge in stages can appear, extra reinforcement of 5 φ16 bars are generally placed in Sweden on both sides of the cross section in the newer part, with a 200 mm cc-distance. This means that in a real case, more reinforcement should be placed in the lower part of the abutment. However, this reinforcement is placed lower than the height levels of the largest crack widths in the model, and when the reinforcement is included, the maximum characteristic crack width is only reduced to 0.32 mm.

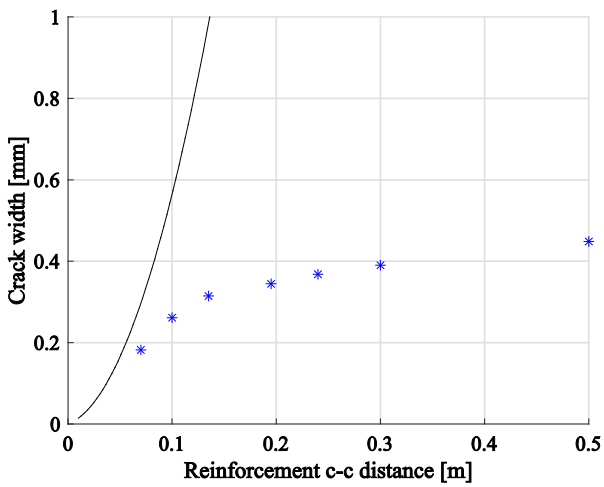

Fig. 4.15. Characteristic crack widths according to non-linear analyses (stars) and crack widths calculated using Eqs. (2.1–2.3) and stresses from linear elastic analyses (line).

Table 4.4. Comparison of crack widths in non-linear analyses, reinforcement required to obtain the same crack widths using the conventional design method and the factor describing the difference in reinforcement amounts.

CC-distance in non-linear analysis [mm]	**70**	**100**	**135**	**195**	**240**	**300**	**500**
Char. crack width in non-linear analysis [mm]	0.18	0.26	0.31	0.34	0.37	0.39	0.45
Required cc to obtain same crack width with conventional method [mm]	55	68	75	79	82	84	92
Factor describing difference in reinforcement amount	1.3	1.5	1.8	2.5	2.9	3.6	5.4

Not only is the crack widths considered unacceptable when the minimum reinforcement amount according to Eq. (2.4) is used. In fact, all the obtained maximum characteristic crack widths are larger than the strictest demand on crack widths in Swedish bridges, i.e. 0.15 mm. Therefore, cracks which are unacceptably wide could form in Swedish portal frame bridges due to the investigated restraint effects. As stated in section 4.4, this is also likely occurring, but it is not, to the author's knowledge, considered to be a major issue for Swedish bridges, although restraint effects are known to cause cracking, see e.g. Table 4.2. Possibly, this is explained by the safety margins added both to the load values and to the crack widths resulting from the analyses, and by disregarding creep in the analyses.

Fig. 4.15 and Table 4.4 show that the reinforcement amount does not influence the crack widths in restraint situations as strongly as in non-restraint situations. This was also indicated in section 4.5.1. One reason for this is that when the reinforcement ratio is increased, the stiffness is also increased, which in turn increases the restraint and also the crack widths. Another possible explanation is that in this type of restraint situation, the restraining edge could be significantly limiting the widths of the cracks. This is suspected as the cracks cannot propagate over the edge, due to the structural part on the other side of the edge being in compression. The small influence of the reinforcement amount can also be seen by observing the crack pattern in the abutments, which are relatively similar. In the seven analyses, three cracks formed in the abutments in all cases except for when the cc-distance was 70 mm, in which case five cracks formed. The crack patters for the cases with φ16 cc 500 mm and 70 mm are shown in Fig. 4.16.

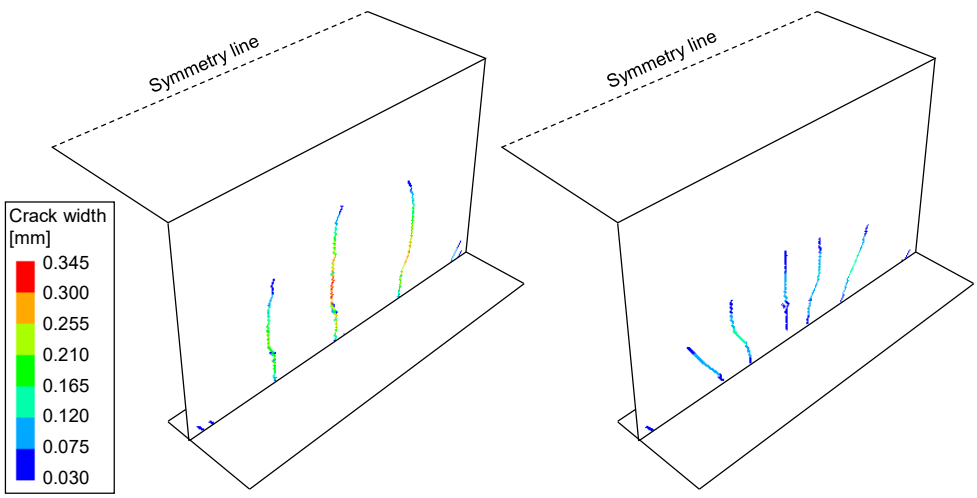

Fig. 4.16. Crack pattern in portal frame bridge with reinforcement φ16 cc 500 mm (left) and φ16 cc 70 mm (right) when having been subjected to characteristic loads which thereafter were reduced to quasi-permanent load values. The given crack widths have not been recalculated to characteristic values.

In order to evaluate the conclusion regarding the influence of the reinforcement ratio on the maximum crack widths, these results were compared with corresponding results in tests and analyses of base restrained walls. The comparison is presented in Table 4.5, which shows reinforcement ratios and maximum crack widths for tests of base restrained walls presented in Kheder (1997) and Micallef et al. (2017), and analyses of the same structures presented in paper V. Ratios of the crack widths are also presented for both analysis results and test results. These ratios thereby describe to what degree the increase in reinforcement affected the maximum crack widths. Analysis results of portal frame bridges with similar reinforcement amounts taken from Table 4.4 are also included in the comparison.

Table 4.5. Comparison of ratios for maximum crack widths in tests and analyses with different reinforcement amounts. Test results are taken from Kheder (1997) and Micallef et al. (2017), and the analyses are performed within this study, presented in paper V and in section 4.5.2.

Structure	Reinforcement ratio [%]	Maximum crack width, test [mm]	Ratios tests	Maximum crack width, analysis [mm]	Ratios analyses
Kheder 1E1	0.20	0.48	1.92	0.63	1.80
Kheder 1E2	0.80	0.25		0.35	
Kheder 2E1	0.20	0.62	1.55	0.65	1.12
Kheder 2E2	0.80	0.40		0.58	
Portal frame bridge cc 500	0.20			0.45	1.45
Portal frame bridge cc 135	0.74			0.31	
Micallef 4	0.48	0.40	1.67	0.28	1.75
Micallef 3	0.74	0.24		0.16	
Portal frame bridge cc 240	0.42			0.37	1.19
Portal frame bridge cc 135	0.74			0.31	

The ratios obtained with the test results from Kheder (1997) are larger than the corresponding ratios for the analysis results recreating the tests, as well as the portal frame bridges with similar reinforcement ratios. However, the ratio value varies significantly both between the comparisons based on test results and analysis results, indicating that the difference between test and analysis ratios could be due to random variations. The ratio obtained with test results from Micallef et al. (2017) is slightly smaller than the corresponding analysis ratio, while the corresponding ratio calculated from the portal frame bridges with similar reinforcement ratios is significantly smaller. In conclusion, the influence of the reinforcement amount on the crack widths is similar in analyses presented in paper V and tests presented in Kheder (1997) and Micallef et al. (2017), to what was found in the portal frame bridges. The slightly smaller influence of reinforcement found in the analyses of portal frame bridges could possibly be explained by e.g. the same number of cracks forming in the analyses of portal frame bridges used for comparison in Table 4.5, and the different width to height ratio of the abutments, compared to the base restrained walls.

Fig. 4.17 shows the maximum characteristic crack widths in different steps of the analyses. The graphs show how the maximum crack width develops under loading up to characteristic load and unloading to the quasi-permanent load level. The difference in strain between abutment and foundation, shown on the horizontal axis in the figure, is caused by both shrinkage and thermal action. It can be seen in Fig. 4.17 that the crack widths did not increase linearly with the increasing restrained strain, as was suggested in Eurocode 2-3 (CEN, 2006). The reason for the crack widths not being proportional to the applied restraint loads is likely the reduction of restraint that occurs as the structure cracks. The effect of reducing the thermal action from its characteristic value to the quasi-permanent value is also visible in the figure.

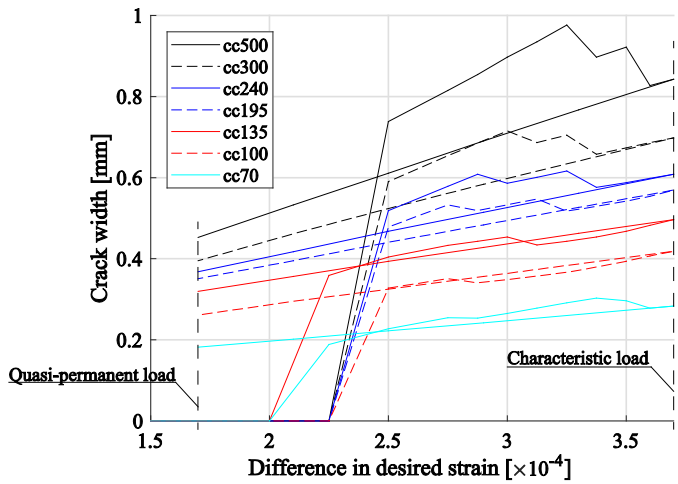

Fig. 4.17. Development of crack widths in analyses of cracking in the lower part of the abutment in portal frame bridges. The horizontal axis shows the corresponding temperature difference between abutment and foundation, i.e. the combined effect of shrinkage and thermal action.

The fact that the same number of cracks appear in all of the analyses except one indicates that the cracks in these cases are formed by the restraining edge and not by the restraint caused by the reinforcement. These three cracks can thus be considered primary cracks, and the two extra cracks in the analysis with cc 70 mm could correspond to secondary cracks, according to the definition in Schlicke and Tue, (2015), as they are likely caused by the reinforcement. However, it can be seen by observing the reductions in crack width appearing in Fig. 4.17 that the second and third cracks form earlier in the analyses with more reinforcement. E.g. in the analysis with cc 100 mm, the third crack appeared already for a difference in strain of $2.9 \cdot 10^{-4}$, while in the analysis with cc 500 mm, the third crack formed at a difference in strain of $3.6 \cdot 10^{-4}$.

It should also be noted that in many of the analyses, the largest crack width appears before the largest restraint load is applied. This indicates that the crack width for quasi-permanent action would have been larger, if the load had not been increased all the way to the characteristic value prior to the load reduction. In the case of cc 500 mm in Fig 4.17, the largest quasi-permanent crack width would have been obtained if the load increase was stopped before the formation of the second crack, at a desired strain difference of $3.25 \cdot 10^{-4}$. This can also be understood as since the formation of additional cracks reduces the stiffness of the structure, the largest stiffness of a cracked structure is obtained when only one crack is present.

An investigation of the effect of changing the width of the bridge was made also in this case. The analysis model with reinforcement cc 300 mm was used, and the width was changed from 10 m to 5 m and 15 m, respectively. A comparison of the results from using both non-linear analysis and the conventional design method is shown in Table 4.6. The comparison shows that increasing the width of the bridge lead to a slight decrease of the factor describing the difference in reinforcement amount, which is similar to what was found in the corresponding investigation in section 4.5.1.

Table 4.6. Comparison of results when the width of the bridge was varied. All analyses were made with reinforcement cc 300 mm.

Bridge width [m]	**5**	**10**	**15**
Number of vertical cracks	1	3	3
Characteristic crack width in non-linear analysis [mm]	0.25	0.39	0.51
Tensile stress used in conventional crack width calculation [MPa]	2.2	2.7	2.9
Required cc to obtain same crack width with conventional method [mm]	74	84	95
Factor describing difference in reinforcement amount	4.1	3.6	3.2

4.5.3 Discussion on comparison of crack widths

The comparisons between the reinforcement amounts required for limiting crack widths to certain values when using the two different analysis methods show that the non-linear analysis consistently rendered significantly smaller reinforcement requirements. However, the factor describing the difference in required reinforcement is in the range of 1.3–4.1, which shows that there were large variations in the results.

It was found that the reinforcement amount used in the non-linear analyses has a large impact on the factor, as adding reinforcement has a smaller influence on crack widths in the non-linear analyses than in the conventional method. It was also found that the width of the bridge affects the factor value, as a wider structure rendered a smaller factor. This can seem unexpected, as the restraint is reduced when cracks form, and there are more cracks in the wider bridge. However, the results of this study indicate that the initial restraining conditions have a larger effect on the cracking, as the cracks were significantly wider when the width of the bridge was increased.

These results show that a relation between the conventional design method and the non-linear analysis results will be difficult to determine, as it will be dependent on several factors, e.g. the reinforcement amount and the geometry of the structure. As can be seen in Fig. 4.17, the crack width changes non-linearly during the crack development stage, and the load magnitude will therefore also affect the factor value.

It was also seen in Fig. 4.17 that the formation of a single new crack can have a large impact on the maximum crack width. Therefore, the factor value can be very different depending on whether one extra crack appears or not. In order for the factor to be accurate, the exact number of cracks in the structure must be anticipated, which will be difficult to achieve. The conservative solution would be to assume only one crack forming, or possibly one crack forming within a certain length of the wall. However, a more extensive study on e.g. the effect of geometrical variations and reinforcement placement is needed before any further conclusions can be drawn. Finally, as the study indicates that the reinforcement amount has a limited influence on the crack widths, it could in some cases be more effective to limit the degree of restraint in the structure by e.g. limit the abutment width to height ratio, than to add extra reinforcement.

5 Summary of appended papers

Paper I – Comparison of Models for Design of Portal Frame Bridges with regard to Restraint Forces

Stresses caused by the thermal load case in Eurocode describing temperature differences between structural parts were investigated. Calculations were performed for a simple portal frame bridge geometry using different model types, and the results show that the load case, such as it was interpreted in the paper, renders large stresses in the transversal direction, if this direction is included in the structural model used for design. The design methods tested did not take the reduction of stresses due to cracking into account, and it was suggested that this, as well as the thermal load case itself, should be investigated further.

Paper II – Simulation of thermal load distribution in portal frame bridges

Thermal simulations were performed using a 2D FE-model of a bridge cross section, which showed that temperature differences can occur between bridge deck and abutments in portal frame bridges due to variations in ambient climate. The study showed that temperature differences can develop between the bridge deck and abutments, and that the temperature changes gradually in the corner region. The gradual change in temperature resulted in smaller restraint stresses compared to the case with an abrupt temperature change. Also, a parametric study was performed in order to investigate which parameters had the largest influence on the temperature difference between the structural parts. It was found that the most significant parameters were the cross-sectional height of the bridge deck, the asphalt heat conductivity and the cross-sectional height of the abutment.

Paper III – Validation of Temperature Simulations in a Portal Frame Bridge

The model for temperature simulation used in paper II was validated for use in portal frame bridges. Temperature measurements were made in 12 locations in a bridge cross section during a 12-month-period, and the validation was done by comparing simulated temperature with the measured temperature values. The results showed that at specific points in time, the temperature difference between the bridge deck and the

abutment differed up to 1.5°C between measurements and simulation. However, the mean values over time agreed well. Therefore, it was recommended that a 1.5°C safety margin is added to extreme values determined using the model, while no safety margin is required for mean values over time.

Paper IV – Spatial Temperature Differences in Portal Frame Bridges

The model used in papers II and III was used to determine characteristic and quasi-permanent load values for the load case describing temperature differences between structural parts in portal frame bridges. The load values were determined using eight data series from different parts of Sweden, and the suggested values were therefore expected to be valid in Swedish climate conditions. However, for three out of four types of temperature differences investigated, a correlation was found with aspects of air temperature variations, which can be used in the future to estimate load values in other locations. For the forth load case, describing the situation when the bridge deck is warmer than the abutment, no simple correlation was found. This is possibly explained by other parameters, such as solar radiation, having a larger impact on the result in this case.

Paper V – Crack widths in base restrained walls subjected to restraint loading

A model for analysis of cracking in reinforced concrete base restrained walls was validated by comparing analysis results with results from tests performed in previous research. The results showed that the model tended to overestimate cracking, but if the thermal stresses caused by the hardening process were disregarded, the model risked to underestimate the resulting crack widths. A sensitivity study was also made, which e.g. showed that the introduction of a bond-slip relation is necessary in order to describe cracking realistically in walls with a high reinforcement ratio.

Paper VI – Crack widths in portal frame bridges subjected to restraint effects

The model used in paper V was developed further in order to analyze cracking in portal frame bridges. The load case developed in paper IV was used as the thermal action in the analyses, and the resulting crack widths were compared with results obtained from (1) not including the effect of stress reduction due to cracking and (2) using an interpretation of the Eurocode thermal load case while not including the stress reduction. The study showed that for the specific geometry used, both the new load definition and the inclusion of stress reduction due to cracking lead to significant reductions of the reinforcement required for crack width limitation.

6 Conclusions

The main conclusions from this dissertation are presented below.

- Differences in temperature between structural parts do occur in portal frame bridges, and these thermal actions should be included in design, in order not to underestimate the restraint effects in the structure.
- The temperature varies spatially in the corner regions of the bridges and in the lower part of the abutments. In the rest of the structure, the temperature generally only varies over the cross-sectional height, and not along the system line. By considering the gradual change of temperature in the corner region and in the lower part of the abutment in the load case, the resulting stresses become smaller, compared to when using the conservative interpretation of the present Eurocode load case. Also, the largest stress values appear in more correct locations.
- The model for temperature simulations used in the study has good accuracy and acceptable precision, in terms of temperature differences between structural parts in portal frame bridges.
- The load values shown in Fig. 3.8 are suggested to be used for the load case describing temperature differences between structural parts in design of portal frame bridges in Swedish climate conditions. The load values were determined using an unfavorable geometry, and the load values chosen are based on the simulation with the most unfavorable weather data.
- The temperature differences between abutment and foundation were found to correlate with the difference between mean temperature in January and July. Also, the temperature difference for the abutment being warmer than the bridge deck was found to correlate with the difference between maximum and minimum temperature during January. Therefore, the air temperature variation over the year can give an indication of reasonable load values that can be expected at specific locations. However, no simple correlation was found between the air temperature and the case when the bridge deck is warmer than the abutment.
- The length of the transition zone in the frame corner is in the suggested load cases 0.65 m both in vertical and horizontal direction along the system line of

the structure. It can be considered to be independent of the thicknesses of the structural parts, and of the tapering of the frame corner. The transition zone between abutment and foundation is suggested to cover the distance from the vertical center of gravity of the foundation to 0.3 m above the ground level below the bridge, and is also found to be independent of the thickness of the abutment.

- The model for analysis of cracking was verified by comparing results with tests performed on base restrained walls, and it was shown that the model tended to overestimate cracking. However, thermal stresses developing during the hardening can cause the cracking to be larger than predicted by the model, if not included in the analyses. As these stresses are often neglected in design calculations, this was considered as acceptable.
- If the reduction of restraint due to cracking is not accounted for in design, it is likely that the resulting stresses will be significantly overestimated.
- Cracking due to spatial temperature differences is unlikely in the bridge deck of portal frame bridges. In the top of the abutment, the crack widths can be larger than the accepted limit, especially if the abutment is thinner than the bridge deck. The largest cracks are however likely to form in the lower part of the abutment and possibly also in the foundation.
- When cracking in base restrained walls and portal frame bridges is caused by restraint effects, the crack widths do not increase proportionally with the restraint effect. The reason for this is that the increase in crack width is reduced when new cracks form, as the structural stiffness is reduced by the formation of every new crack.
- Crack widths in portal frame bridges have a weaker dependency on the reinforcement amount than anticipated with the Eurocode 2-1-1-equations for crack width calculation, which were developed for non-restraint cases. This is likely explained by the increased reinforcement amount increasing the stiffness of the structure, which in turn increases the restraint. Also, the restraining edge is itself limiting the crack widths, as the structure is in compression on the other side of the edge and the cracks thus will not extend beyond it.
- The minimum reinforcement amount was not sufficient in order to limit crack widths, when the suggested thermal load case and shrinkage was applied in the developed FE-analysis model which describes cracking. As increasing the reinforcement amount has a limited influence on the resulting crack widths, it could be more effective to limit the degree of restraint in design situations, by e.g. limiting the abutment width to height ratio.

6.1 Further research needs

The development and verification of the model for thermal simulations enables extended studies of the temperature differences between structural parts of bridges. Some possibilities regarding the model for temperature simulations are listed below.

- To investigate other bridge types or special geometrical cases of portal frame bridges.
- To develop load cases for other geographic areas. However, if the climate in the chosen area is profoundly different, a new verification of the simulation model could be required, as the climate and heat transfer aspects could be of different importance.
- To determine local load values for Sweden, instead of national. The present study indicates that the temperature difference between abutment and foundation is smaller in the parts of the country where the seasonal temperature variations are small. The temperature difference between abutment and foundation could therefore likely be reduced in many coastal areas, and in the southern part of the country in general. As radiation data is measured in only a few locations in the country, calculated radiation data could be used in future analyses.

Also, the study of cracking in portal frame bridges could be extended, and the following investigations are possible:

- To investigate cracking in existing bridges, and evaluate if cracks can be connected to the restraint effects investigated in this study. Such results could possibly also be used to confirm the reliability of the analysis model used in this study.
- To perform a parametric study on the crack widths, focusing on the influence of the geometry of the structure.
- To establish a relation between results obtained using linear elastic analyses used in design and the results from non-linear analyses, in order to calibrate the common design using the more accurate non-linear model.

7 References

ACI Committee 207 (1990), *Effect of Restraint, Volume Change, and Reinforcement on Cracking of Mass Concrete*, ACI Materials Journal, Vol. 87, pp. 271–295.

ACI Committee 224 (1998), *Causes, Evaluation, and Repair of Cracks in Concrete Structures.* American Concrete Institute.

ACI Committee 224 (2001), *Control of Cracking in Concrete Structures,* American Concrete Institute.

Balázs, G.L. (2013), *Design for SLS according to fib Model Code 2010,* Structural Concrete, Vol. 14, No. 2, pp. 99–123.

Bamforth, P, Denton, S. & Shave, J. (2010), *The development of a revised unified approach for the design of reinforcement to control cracking in concrete resulting from restrained contraction*, Institution of Civil Engineers, ICE Research project 0706.

Beeby, A.W. (1983), *Cracking, Cover and Corrosion of Reinforcement*, Concrete International, Vol. 5, No. 2, pp. 35–40.

Boverket (2015), *Boverkets författningssamling, EKS10*, BFS2015:6, Boverket.

Branco, F. & Mendes, P. (1993), *Thermal Actions for Concrete Bridge Design*, Journal of Structural Engineering, Vol. 119, No. 8, pp. 2313–2331.

Bretz, S, Akbari, H. & Rosenfeld, A. (1997), *Practical Issues for Using Solar-Reflective Materials to Mitigate Urban Heat Islands*, Atmospheric Environment, Vol. 32, No. 1, pp. 95–101.

Brown, M, Sellers, G, Folliard, K.J. & Fowler, D.W. (2001), *Restrained Shrinkage Cracking of Concrete Bridge Decks: State-of-the-Art Review*, Report No. FHWA/TX-0-4098-1, Center for Transportation Research, University of Texas, Austin, TX, United States.

Bureau of Reclamation (1942), *Concrete Manual*, United States Department of the Interior, 4th Edition. Denver, CO, United States.

Bygginovationen (2010), *Delrapport: Bro*, Bygginovationen.

CEB (Euro-International Committee for Concrete) (1985), *Bulletin d'information no 158-E, Design Manual on Cracking and Deformations,* Lausanne, Switzerland.

CEN (European Committee for Standardization) (1996), *Background document to ENV 1991-2-5: Thermal actions*, Draft: February 1996.

CEN (European Committee for Standardization). (2003), *Actions on structures - Part 1-5: General actions – Thermal actions*. Eurocode 1, Brussels, Belgium.

CEN (European Committee for Standardization). (2005a), *Design of concrete structures - Part 1-1: General rules and rules for buildings*. Eurocode 2, Brussels, Belgium.

CEN (European Committee for Standardization). (2005b), *Design of concrete structures – Part 2: Concrete bridges – Design and detailing rules*. Eurocode 2, Brussels, Belgium.

CEN (European Committee for Standardization). (2006), *Design of concrete structures – Part 3: Liquid retaining and containment structures*. Eurocode 2, Brussels, Belgium.

CEN (European Committee for Standardization). (2002), *Basis of structural design*. Eurocode 0, Brussels, Belgium.

Duffie, J. & Beckman, W. (2006), *Solar Engineering of Thermal Processes,* John Wiley & Sons, Inc, Hoboken, NJ, United States.

Elbadry, M. & Ghali, A. (1995), *Control of Thermal Cracking of Concrete Structures*, ACI Structural Journal, Vol. 92, No. 4, pp. 435–450.

Engström, B. (2014), *Restraint cracking of reinforced concrete structures*, Chalmers University of Technology, Gothenburg, Sweden.

Eriksson, M. & Fritzson, E. (2014), *Crack Control of Extended Concrete Walls,* Master's thesis, Chalmers University of Technology, Report 2007:10, Edition 2014, Gothenburg, Sweden.

Farra, B. (1995), *Influence de la résistance du béton et de son adhérence avec l'armature sur la fissuration,* PhD dissertation, Swiss Federal Institute of Technology, Lausanne, Switzerland.

fib (Fédération internationale du béton) (2013), *fib Model Code for Concrete Structures 2010*, Wilhelm Ernst & Sohn, Berlin, Germany.

François, R, Khan, I, Vu, N.A, Mercado, H. & Castel, A. (2012), *Study of the impact of localised cracks on the corrosion mechanism*, European Journal of Environmental and Civil Engineering, Vol. 16, No. 3–4, pp. 392–401.

Frosch, R.J, Blackman, D.T. & Radabaugh, R.D. (2003), *Investigation of Bridge Deck Cracking in Various Bridge Superstructure Systems*, Publication no. FHWA/IN/JTRP-2002/25, Joint Transportation Research Program, Indiana Department of Transportation and Purdue University, West Lafayette, IN, United States.

Ghali, A. & Favre, R. (1994), *Concrete Structures: Stresses and Deformations,* E&FN Spon, London, United Kingdom.

Goforth, M.A, Gilchrist, G.W. & Sirianni, J.D. (2002), *Cloud Effects on Thermal Downwelling Sky Radiance*, Proceedings of SPIE conference AeroSense, Orlando, FL, United States.

Gylltoft, K. (1983), *Fracture Mechanics Models for Fatigue in Concrete Structures,* Luleå University of Technology, Luleå, Sweden.

Halvorsen, G.T. (1993), *Troubleshooting Concrete Cracking During Construction*, Concrete Construction, October 1993.

Hillel, D. (2004), *Introduction to environmental soil physics*, Academic Press, San Diego, CA, United States.

Idso, S.B. & Jacksson, R.D. (1969), *Thermal Radiation from the Atmosphere*, Journal of Geophysical Research, Vol. 74, No. 23, pp. 5397–5403.

Incropera, F.P, Dewitt, D.P, Bergman, T.L. & Lavine, A.S. (2007), *Fundamentals of Heat and Mass Transfer,* John Wiley & Sons, Hoboken, NJ, United States.

Jaccoud, J-P. (1987), *Minimum reinforcement for control of cracking in concrete structures,* PhD dissertation, Swiss Federal Institute of Technology, Lausanne, Switzerland.

Jaccoud, J-P. (1997), *Cracking under long term loads or imposed deformations*, CEB Bullettin 235, pp. 143–155.

Jaccoud, J-P, Farra, B. & Leclercq, A. (1996), *Improvement of existing codes for their application to crack control of HSC/HPC structures*. Proceedings of the 4th International Symposium on Utilization of High-strength/High Performance Concrete, Paris.

Jansson, A. (2011), *Effects of Steel Fibres on Cracking in Reinforced Concrete,* PhD dissertation, Chalmers University of Technology, Gothenburg, Sweden.

Jansson, A, Flansbjer, M, Löfgren, I, Lundgren, K. & Gylltoft, K. (2012), *Experimental investigation of surface crack initiation, propagation and tension stiffening in self-compacting steel-fibre-reinforced concrete*, Materials and Structures, Vol. 45, pp. 1127–1143.

Jokela, J. (1984), *Behaviour and Design of Concrete Structures under Thermal Gradients*, Nordic Concrete Research, No. 3, pp. 100–128.

Kheder, G.F. (1997), *A New look at the control of volume change cracking of base restrained concrete walls*, ACI Structural Journal, Vol. 94, No. 3, pp. 262–271.

Kheder, G.F, Al-Rawi, R.S. & Al-Dhahi, J.K. (1994), *A study of the behaviour of volume change cracking in base restrained concrete walls*, Materials and Structures, Vol. 27, No. 7, pp. 383–392.

Kianoush, M.R, Acarcan, M. & Ziari, A. (2008), *Behavior of base restrained reinforced concrete walls under volumetric change*, Engineering Structures, Vol. 30, pp. 1526–1534.

Krauss, P.D. & Rogallla, E.A. (1996), *Transverse Cracking in Newly Constructed Bridge Decks*, National Cooperative Highway Research Program (NCHRP), Report no. 380, Wiss, Janney, Elstner Associates Inc, Northbrook, IL, United States.

Kreith, F. (1973), *Principles Of Heat Transfer,* Intext Educational Publishers, New York, NY, United States.

Larsson Ivanov, O. & Gottsäter, E. (2019), *Framtagande av temperaturlaster i broar med hjälp av allmänt tillgängliga klimatdata*, *TVBK; Report no. 3071,* Division of Structural Engineering, Lund University, Lund, Sweden.

Larsson, O. (2009), *Modelling of Temperature Profiles in a Concrete Slab under Climatic Exposure*, Structural Concrete, Vol. 10, No. 4, pp. 193–201.

Larsson, O. (2012), *Climate related thermal actions for reliable design of concrete structures*, PhD dissertation, Division of Structural Engineering, Lund University, Lund, Sweden.

Ljungkrantz, C, Möller, G. & Petersons, N. (1994), *Betonghandbok-material*, Svensk byggtjänst, Stockholm, Sweden.

Matinmanesh, H. & Kianoush, M.R. (2013), *A Parametric Study on Temperature Cracking in Base Restrained Reinforced Concrete Walls*, Annual Conference – Canadian Society for Civil Engineering, Montreal, Canada.

Micallef, M, Vollum, R.L. & Izzuddin, B.A. (2017), *Crack development in transverse loaded base-restrained reinforced concrete walls*, Engineering Structures, Vol. 143, pp. 522–539.

Nesset, J. & Skoglund, S. (2007), *Reinforced Concrete Subjected to Restraint Forces,* Master's thesis, Chalmers University of Technology, Gothenburg, Sweden.

Otieno, M.B, Alexander, M.G. & Beushausen, H-D. (2010), *Corrosion in cracked and uncracked concrete – influence of crack width, concrete quality and crack reopening*, Magazine of Concrete Research, Vol. 62, No. 6, pp. 393–404.

Poppe, J.B. (1981), *Factors Affecting the Durability of Girder Bridge Decks*, Calofornia Dept. of Transportation: Division of Transportation Facilities Design, Sacramento, CA, United States.

Portland Cement Association (1970), *Durability of Concrete Bridge Decks*, Skokie, IL, United States.

Quinn Brewster, M. (1992), *Thermal Radiative Transfer and Properties,* Wiley-Interscience, New York, NY, United States.

Saadeghvaziri, M. & Hadidi, R. (2005), *Transverse Cracking of Concrete Bridge Decks: Effects of Design Factors*, Journal of Bridge Engineering, Vol. 10, No. 5, pp. 511–519.

Schlicke, D. & Tue, N.V. (2015), *Minimum Reinforcement of Concrete Members regarding Hardening Caused Stresses and Member Dimensions*, Structural Concrete, Vol. 16, No. 2, pp. 221–232.

Schmitt, T.R. & Darwin, D. (1995), *Cracking of Concrete Bridge Decks*, Report no. K-TRAN: KU-94-1, University of Kansas, Lawrence, KS, United States.

Soroushian, P. & Choi, K-B. (1989), *Local Bond of Deformed Bars with Different Diameters in Confined Concrete*, ACI Structural Journal, Vol. 86, No. 2, pp. 217–222.

Stoffers, H. (1978), *Cracking due to shrinkage and temperature variations in walls*, Heron, Vol. 23, No. 3, pp. 1–68.

Sundberg, J. (1991), *Termiska egenskaper i jord och berg*, Statens geotekniska institut, Linköping, Sweden.

Swinbank, W.C. (1963), *Long-wave Radiation from Clear Skies*, Quarterly Journal of the Royal Meteorological Society of London, Vol. 89, pp. 339–348.

The Concrete Society (1992), *Non-Structural Cracks in Concrete,* Technical Report No. 22, London, United Kingdom.

Threlkeld, J.L. (1970), *Thermal Environmental Engineering,* Prentice Hall, Englewood Cliffs, NJ, United States.

Trafikverket (2011a), *Trafikverkets författningssamling TRVFS 2011:12 – Trafikverkets föreskrifter om ändring i Vägverkets föreskrifter (VVFS 2004:43) om tillämpningen av europeiska beräkningsstandarder,* ISSN 2000-5458, Borlänge, Sweden.

Trafikverket (2011b), *TRVR Bro 11 – Trafikverkets tekiska råd Bro*, Publication no. 2011:086, ISBN: 978-91-7467-154-4.

Trafikverket (2016a), *Krav Brobyggande*, Publication no. TDOK 2016:0204, Version 1.0.

Trafikverket (2016b), *Råd Brobyggande*, Publication no. TDOK 2016:0203, Version 1.0.

Trafikverket (2018), BaTMan, https://batman.trafikverket.se/externportal; 2019-09-24.

Vägverket (1993), *BRO, Handbok för broinspektion*, Tabergs Tryckeri AB, Jönköping, Sweden.

Vägverket (1994), *BRO 94 – del 4. Betongkonstruktioner*. Publication 1994:4.

Vägverket (2004), *Vägverkets allmänna tekniska beskrivning för nybyggande och förbättring av broar – Bro 2004,* Publication 2004:56, ISSN 1401-9612.

Zangeneh Kamali, A, Svedholm, C. & Johansson, M. (2013), *Effects of restrained thermal strains in transversal direction of concrete slab frame bridges,* KTH Royal Institute of Technology, Stockholm, Sweden, ISSN 1103-4289.

Zhou, Y, Gencturk, B, Willam, K. & Attar, A. (2015), *Carbonation-Induced and Chloride-Induced Corrosion in Reinforced Concrete Structures*, Journal of Materials in Civil Engineering, Vol. 27, No. 9.